



## Durham E-Theses

---

### *Computer simulation of diesel and diesel additives*

Nasi, Matteo

#### **How to cite:**

---

Nasi, Matteo (2007) *Computer simulation of diesel and diesel additives*, Durham theses, Durham University. Available at Durham E-Theses Online: <http://etheses.dur.ac.uk/2401/>

#### **Use policy**

---

The full-text may be used and/or reproduced, and given to third parties in any format or medium, without prior permission or charge, for personal research or study, educational, or not-for-profit purposes provided that:

- a full bibliographic reference is made to the original source
- a [link](#) is made to the metadata record in Durham E-Theses
- the full-text is not changed in any way

The full-text must not be sold in any format or medium without the formal permission of the copyright holders.

Please consult the [full Durham E-Theses policy](#) for further details.

# Computer Simulation of Diesel and Diesel Additives

MATTEO NASI

Department of Chemistry

University of Durham

England

January 2007

The copyright of this thesis rests with the author or the university to which it was submitted. No quotation from it, or information derived from it may be published without the prior written consent of the author or university, and any information derived from it should be acknowledged.

A thesis submitted in partial fulfillment of the requirements for the degree of

MASTER OF SCIENCE



# Abstract

## Computer Simulation of Diesel and Diesel Additives

Matteo Nasi

The formation of *n*-alkane (paraffin) wax crystals in diesel fuel in winter time is an important problem for many oil industries. This thesis investigates the possibilities of making a simulation model, which can be used to study the behavior of diesel fuel, and can be used to investigate crystallization. Initial work focused on finding a suitable molecular mechanics force field. Hexane molecules were modeled with three different force field and the TraPPE force field was chosen. A model of a liquid diesel fuel was produced composed of 78.7 % of a branched alkane solvent (2,4,6,10 tetramethyl dodecane) plus a distribution of *n*-alkanes from C<sub>10</sub> to C<sub>26</sub>. After technical problems, due to the inhomogeneity of the system leading to a formation of clusters molecules with gaps between them, equilibration of a model liquid diesel was achieved starting from an initial gas phase simulation. Calculated liquid density was in good agreement with experiment. Volume, total energy, enthalpy, radial distribution functions and dihedral angle distributions of the solvent molecules all confirmed equilibration of the model diesel. A crystallization inhibitor consisting of a random co-polymer of ethylene vinyl acetate, EVA, was simulated. Starting from an extended configuration led to the formation of a coiled chain in the gas phase. The chain was added to the liquid diesel model and it was found that the diesel can be considered as a good solvent for EVA polymer, with the radius of gyration for EVA increasing slightly in the diesel. An orthorhombic structure with  $P_{bcm}$  space group of tricosane (C<sub>23</sub>H<sub>48</sub>) was built and incorporated into the liquid diesel and the liquid diesel / EVA models. In these models it was found that edges of the crystal started to melt into the liquid diesel as a function of time. The EVA was found to migrate to the surface of the crystal.

# Acknowledgments

March 12, 2007

I have a great many people to thank for the help and support I have received in this year. Firstly, I would like to thank Infineum Ltd. and particularly Dr Robert Tack for funding the grant that supported this work and The University of Durham providing the computing resources essential for this kind of research.

My supervisor, Dr Mark Wilson, who support me from the beginning when I started without any knowledge of the subject. His door was all the time open, especially in the hard moments when the simulations went wrong. He made me realize what research is about and give me very important feedback for the future.

I want to say thank you to the people that I met here in Durham, and some of them become friends, Dr Zak Hughes and Mr Jorge Pelaez that helped me when I started. From the ITS department I great thanks are due to Mr Neil Millar who gave me considerable help with system operator problems. To Mr Musie Buyene, Dr Alex Trottier, Dr Sabastian Palucha with whom I share laughs and hard moments and they were able to give me good academic and personal support. To Musie that was very patient and supportive in my learning journey, particularly in some difficult moment we overcame together.

To the other people I met in Durham in a none academic environment, like Chaya, Mauricio, Maria Jose, Maria The Graek, Tiffany, Corina with whom I pass very nice evenings in pubs chilling out.

To my Elif, that love and support me all the time and all her friends in Cambridge that made me feel at home.

To all my family, my mother, brother, grandmother, Granfher that help me from Italy.

# Declaration

The material contained within this thesis has not previously been submitted for a degree at the University of Durham or any other University. The research reported within this thesis has been conducted by the author unless indicated otherwise.

The copyright of this thesis rests with the author. No quotation from it should be published without his prior written consent and information derived from it should be acknowledged.

Matteo Nasi

January 2007

# Dedication

To my Dad

# Contents

<b>1</b>	<b>Introduction</b>	<b>15</b>
1.1	Project aim . . . . .	15
<b>2</b>	<b>Diesel fuel and wax crystallization</b>	<b>15</b>
2.1	Consideration for Wax Crystal Modifiers . . . . .	17
2.1.1	Association with the wax . . . . .	17
2.1.2	Solubility . . . . .	17
2.1.3	Blocking groups . . . . .	17
2.1.4	Ease and cost of production . . . . .	18
<b>3</b>	<b>Previous work on simulation of crystal inhibitors</b>	<b>18</b>
3.1	Molecular Simulation works using a kinetic inhibitors . . . . .	19
3.2	Molecular Simulation works using anti-agglomerants inhibitors . . . . .	21
<b>4</b>	<b>Simulation Method for the Project</b>	<b>23</b>
4.1	Force field models: molecular mechanics . . . . .	23
4.1.1	Introduction . . . . .	23
4.1.2	The anatomy of a molecular mechanics force field . . . . .	24
4.1.3	Bond stretching . . . . .	24
4.1.4	Torsions . . . . .	28
4.1.5	Non bonded interactions . . . . .	32
4.1.6	Different type of force field . . . . .	35
<b>5</b>	<b>Molecular Dynamics Simulation</b>	<b>35</b>
5.1	Introduction . . . . .	35
5.2	Molecular dynamic methods . . . . .	37
5.2.1	Newton's Second Law . . . . .	37
5.2.2	Integration algorithms . . . . .	38
5.2.3	Statistical mechanics . . . . .	40
5.2.4	Molecular dynamics and ensembles . . . . .	41

<b>6</b>	<b>Assessment of force field for hydrocarbons</b>	<b>45</b>
6.1	Different force field for hydrocarbons . . . . .	46
6.1.1	OPLS-UA . . . . .	46
6.1.2	TraPPE (Transferable Potential for Phase Equilibria Force Field) . . . . .	47
6.1.3	NERD . . . . .	49
6.2	A comparison of force field for <i>n</i> -hexane. . . . .	49
6.2.1	The steps required in a MD simulation using hexane as an example . . . . .	51
6.2.2	Result . . . . .	52
6.3	Accurate description of TraPPE-UA force field . . . . .	58
<b>7</b>	<b>Simulation of a model diesel</b>	<b>59</b>
7.1	Results from the model liquid diesel simulation . . . . .	64
<b>8</b>	<b>Wax Crystal Modifier (EVA)</b>	<b>69</b>
8.0.1	Random co-polymers . . . . .	69
8.0.2	Comb type polymer. . . . .	70
8.0.3	Nucleators . . . . .	70
8.1	Characteristics of EVA . . . . .	70
8.2	Force Field Parameters of EVA . . . . .	71
8.3	A property of EVA polymer: radius of gyration . . . . .	76
<b>9</b>	<b>EVA + Diesel</b>	<b>79</b>
9.1	Results for EVA plus diesel . . . . .	82
<b>10</b>	<b>Crystal</b>	<b>83</b>
10.1	<i>n</i> -alkanes crystals . . . . .	83
10.2	C23 crystal . . . . .	83
<b>11</b>	<b>Model Diesel plus Crystal simulations</b>	<b>85</b>
<b>12</b>	<b>Model Diesel plus Crystal plus EVA</b>	<b>88</b>

**13 Conclusion**

**92**

**References**

**94**

## List of Figures

1	Plot of the fraction of hydrate-like water molecules formed within time for an uninhibited (shown as solid line) and inhibited (shown as dashed lines) simulation (Figure 1 of ref. [10] used with permission).	19
2	Radial distribution function for the water-methane system in the uninhibited and inhibited simulation (Figure 2 of ref. [10] used with permission).	20
3	The PA-18 adsorbed on the (100) (shown on left) and (010) surface of an octosane wax crystal. Note that periodic boundary condition have been considered in order to show the inter-lamellar gaps across each surface (Figure 4 of ref. [10] used with permission).	22
4	Top and side view of a system in which three layers of crystal wax were added onto an inhibited surface (Figure 1 of ref. [10] used with permission)	23
5	Comparison of the performance of various functional forms for the stretch energy of CH bond in CH <sub>4</sub> . The “exact curve “ is taken from an electronic structure calculation. (Figure taken from figure 2.1 of reference [14]).	26
6	Comparison of the performance of various functional forms for the angle bending energy of CH <sub>4</sub> ; the “exact curve” form is taken from an electronic structure calculation. (Figure taken from Figure 2.4 of reference [14] )	27
7	Dihedral angle between the atom <i>A,B,C,D</i> .(Figure taken from Figure 2.7 of reference [14]).	28
8	The first three terms in a typical function to model the torsional energy.	31
9	Total energy of torsion of a dihedral angle as a sum of the three terms in equation 11.	32
10	Lennard-Jones Potential. (Figure taken from Chemistry Department Website of Saint Johns University, Minnesota, US).	34

11	Periodic boundary condition. (Figure taken from Figure 2.4 of reference [14]). . . . .	44
12	Dihedral angle distribution functions for angles A-C using the OPLS-UA force field. . . . .	53
13	Dihedral angle distribution functions in hexane for angles A-C using the NERD force field. . . . .	55
14	Dihedral angle distribution functions for angles A-C using the TraPPE force field . . . . .	57
15	The distribution of <i>n</i> -alkanes in a typical diesel up to C26. Data is supplied by Infineum. . . . .	59
16	Snapshot of the model diesel compressed from gas phase towards a liquid, where the molecules have condensed into clusters of diesel liquid leaving gaps between the cluster. . . . .	62
17	A snapshot of the model diesel condensed to liquid state density. Note that molecules wrap round the periodic boundary conditions (density calculated: $0.83 \text{ g cm}^{-3}$ ) . . . . .	63
18	Volume as a function of time for an equilibration run of the model diesel system at 1 atmosphere and 298 K, illustrating compression from an initial low density lattice configuration. . . . .	64
19	Total energy as a function of time for an equilibrium run of the model diesel at 1 atmosphere and 298K, during compression from an initial low density lattice configuration. . . . .	64
20	Radial distribution function of each of the different interaction types in our liquid diesel model. . . . .	66
21	Chemical structure of the solvent, the 2,4,6,10 tetramethyl dodecane showing the dihedral angles . . . . .	67
22	Dihedral angle distribution of different angles of the solvent in our model liquid diesel . . . . .	68

23	An extended EVA chain drawn with Maestro molecular modelling software, before starting the simulation. Notice the random distribution of the vinyl acetate group and the butyl group in the long chain polymer. . . . .	73
24	EVA snapshots from a gas phase MD simulation . . . . .	74
25	EVA snapshots from a gas phase MD simulation . . . . .	75
26	EVA snapshots from a gas phase MD simulations . . . . .	76
27	Radius of gyration squared and $x, y, z$ components plotted against the simulation time. . . . .	77
28	Mean value of the radius of gyration of EVA as an “equilibrated” chain polymer in a gas phase. . . . .	78
29	Snapshot of the model diesel condensed to liquid state density. This snapshot shows unperiodically boxed diesel molecules, so that individual molecules are not split by being wrapped round the periodic boundary conditions. . . . .	79
30	Starting configuration of the system made using our model diesel plus the EVA polymer . . . . .	80
31	Equilibrated system of EVA plus our liquid model diesel: snapshot of the final configuration where the system was unboxed and EVA was shifted at the center of the box . . . . .	81
32	Radius of gyration of the EVA polymer in the liquid diesel solvent plotted as a function of simulation time in ps. . . . .	82
33	Crystal $C_{23}$ before the simulation . . . . .	84
34	Figure of the crystal $C_{23}$ after the simulation (Note atoms at the end of the cell are broken across the periodic boundary conditions). . . . .	84
35	Snapshot after the first simulation (100 steps) of the model liquid diesel and the $C_{23}$ crystal. (Note atoms at the edge of the cell are broken across the periodic boundary conditions). . . . .	86
36	Snapshot after the last simulation in the $NVT$ ensemble of the model liquid diesel and the $C_{23}$ crystal (notice that there are still gaps in the system). $t + \Delta t$ . . . . .	87

37	Snapshot of the model liquid diesel plus the $C_{23}$ crystal after rapid compression at high pressure in the $NpT$ ensemble. . . . .	88
38	Snapshot of the final simulation carried out for the model liquid of diesel plus crystal plus EVA. . . . .	89
39	Snapshot of the final configuration of the $NVT$ simulations described in table 28. . . . .	90
40	Snapshot of the final $NpT$ simulation at 1 atm in order to relax the system (note that now all the gaps between the different components of the system have been filled). . . . .	91

## List of Tables

1	Lennard Jones 12-6 parameters for OPLS-UA force field. . . . .	46
2	1-2 Interaction [Stretch] for OPLS-UA force field. . . . .	47
3	1-3 Interaction [Bend] for OPLS-UA force field. . . . .	47
4	1-2 Interaction [Stretch]. . . . .	47
5	1-3 Interaction [Bend]. . . . .	48
6	Lennard Jones 12-6 parameters. . . . .	48
7	Non-bond interaction in TraPPE and NERD force field. . . . .	49
8	% trans-gauche populations of the three dihedral angles in hexane using the OPLS-UA force field. . . . .	52
9	% trans-gauche populations of the three dihedral angles in hexane using the NERD force field. . . . .	54
10	% Trans-gauche population of the three dihedral angles in hexane using the TraPPE force field. . . . .	56
11	% of linear saturated hydrocarbons in a typical diesel fuel. Data is supplied by Infineum. . . . .	60
12	% of linear saturated hydrocarbons in our model diesel . . . . .	60
13	Parameters of the four simulations of the model liquid diesel from a gas phase to a liquid phase carried out in order to achieve equilibrium in the system. . . . .	63
14	Trans-gauche relative percentages for dihedral angles within the sol- vent in our model liquid diesel. Definition of angles are given in figure 21. . . . .	68
15	1-2 Interaction [Stretch] . . . . .	71
16	1-3 Interaction [Bend] . . . . .	71
17	1-4 Interaction [Torsion] . . . . .	72
18	Lennard Jones 12-6 parameters . . . . .	72
19	Partial charges used in EVA simulation . . . . .	72
20	Summary of the first EVA MD simulations . . . . .	73
21	Parameters of the second EVA gas phase MD simulation. . . . .	78

22	Conditions for a molecular dynamics simulation for EVA plus our model liquid diesel. . . . .	80
23	Molecular dynamic simulation of the system EVA + our liquid model diesel after compressing the system. . . . .	81
24	Unit cell parameters of $C_{23}$ . . . . .	83
25	Parameters of a molecular dynamic simulation of 64 molecules of $C_{23}$ orthorhombic crystal. . . . .	84
26	Parameters of the first series of simulations in $NVT$ ensemble of our liquid model diesel plus the $C_{23}$ crystal. . . . .	85
27	Parameters of a series of simulation in $NpT$ ensemble at high pressure of the model liquid diesel plus the $C_{23}$ crystal. . . . .	87
28	Parameters of $NVT$ ensemble simulations, carried out for the mixture model diesel plus crystal plus EVA. . . . .	89
29	Parameters for $NpT$ simulations of diesel plus crystal plus EVA. . . .	90

# 1 Introduction

## 1.1 Project aim

The project involves collaboration with Infineum UK Ltd., a petroleum additives enterprise. The problem to be addressed concerns the formation of plate-like  $n$ -alkane (paraffin) wax crystals in diesel fuel in winter time. These wax crystals gel the fuel and block the diesel engine fuel filters, preventing the flow of fuel causing the engine to stop or not start. Wax Crystal Modifying (WCM) additives are added to diesel fuel to alter the wax crystal habit into compact prisms that do not gel and form porous filter cakes on fuel filters.

Diesel fuel is a mixture of  $n$ -alkanes, isoalkanes e.g. phytane and trimethyl dodecane, alicyclics e.g. dipentylhexane and alkyl aromatics e.g. dihexyl and diethyl benzene.

This project is designed to gain insights into:

- The structure of diesel fuel.
- The phase separation of  $n$ -alkanes from solution.
- The behavior and structure of WCM additives in diesel fuel.
- The interactions of WCM additives with separating  $n$ -alkane crystals.

In order to provide this understanding we plan to:

- Build molecular models of diesel fuel involving a mixture of low molecular weight hydrocarbons (simulated at the United Atom Model level).
- Model the polymer structure of a typical additive and add it to the diesel fuel model to understand better the behavior of the additive in solution.

## 2 Diesel fuel and wax crystallization

A major problem for both refiners and users of diesel fuel or home heating oil is the behavior of such a fuel in cold weather. Diesel contains varying amounts of  $n$ -alkanes

(generally 10-30 %). When diesel fuel is subjected to low temperatures the higher molecular weight *n*-alkanes become insoluble and precipitate from the fuel as wax crystals.

The cold flow properties of middle distillate are defined by the following three parameters [1].

1. *Cloud Point* (CP) is the temperature at which the crystals first appear. This value is determined by a standard method, ASTM D2500, or differential scanning calorimetry measurements. The cloud point depends on the concentration, the molecular weight of the *n*-alkanes and on the chemical nature of the hydrocarbons matrix.
2. *Pour Point* (PP). As the temperature gets colder, crystal growth continues and a lattice is obtained leading to solidification at the pour point. This value is calculated according to the standardized method ASTM D97.
3. *Cold filter plugging point* (CFPP). CP and PP cannot be directly correlated to the plugging of filters by *n*-alkane crystals, so a third parameter is used, the cold filter plugging point, which corresponds to the plugging of 45  $\mu\text{m}$  filter under standardized cooling conditions (Test EN116).

The presence of solid wax crystals in the fuel can cause blockage of filters and narrow lines in the fuel system, so leading to operational failure of a diesel vehicle. In the past these problems were minimized by the production of diesel fuel with low cloud point or by addition of kerosene. An alternative approach in many parts of the world, is to use chemical additives to improve the low-temperature properties of diesel fuel [2].

These additives have the following possible action:

- Modification of the size and shape of the crystals of *n*-alkanes appearing in the fuel when cooled below its cloud point (PP and CFPP depressants).
- Complete inhibition of wax crystallization depressing the cloud point (CP depressants)

In general these additives are called *Wax Crystal Modifiers* (WCM).

## 2.1 Consideration for Wax Crystal Modifiers

In order to make their use economical, WCM must operate at low concentrations (0.01-0.1%), consequently their structure must be optimized with respect to

1. the ability to associate strongly with the wax,
2. an appropriate solubility in the fuel,
3. appropriate groups to block crystal growth or promote nucleation,
4. ease and cost of production,

as described below.

### 2.1.1 Association with the wax

In order to associate with the wax crystal, part of the additive must be *n*-alkane like. Thus the molecule may have *n*-alkyl substituent or a polyethylene like segment in the polymer backbone.

### 2.1.2 Solubility

If too soluble a growth inhibitor will not adsorb onto the wax, except at high concentration, or a nucleator will not separate before the wax and therefore they will be either ineffective or unacceptably expensive. If too insoluble the additive is likely to separate before the wax, associating with itself and not with the wax. The solubility has to be carefully controlled by the ratio of polar to non-polar groups, of branched alkyl or aromatics to linear alkyl groups and by molecular weight. For high effectiveness WCM must begin to precipitate at the same temperature or just above the temperature at which the wax crystallizes.

### 2.1.3 Blocking groups

These need to be large enough and suitably situated on the adsorbed molecule to inhibit further growth on the face of the wax crystal where the inhibitor is adsorbed. However the blocking group must not inhibit adsorption of the additive onto the wax crystal.

#### 2.1.4 Ease and cost of production

In the past production costs have limited polymers to those produced by free radical methodologies using low cost monomers; for example, ethylene, vinyl acetate,  $\alpha$ -olefins and derivatives such as dialkyl fumarates, alkyl methacrylates or alkyl acrylates. For the future the use of more complex syntheses and/or more expensive raw materials has not been ruled out [3], [4].

### 3 Previous work on simulation of crystal inhibitors

An extensive research effort has been carried out to develop new and better WCM, but progress is limited by a lack of deep understanding of the inhibition mechanisms. What is generally known is that the WCM are surface active, in the sense that they adsorb to the surface of small crystals, and thereby disrupt further growth or aggregation of the crystals.

In order to provide a better understanding of the behaviour of inhibitors, neutron scattering has been carried out [5]- [6]. Moreover, useful information can be gleaned by comparison with anti-freeze proteins [7]- [8].

Dr M. Duffy and Dr P. M. Rodger in the Chemistry Department of the University of Warwick and in the Physics and Astronomy Department of University College London have put considerable effort into understanding the behavior of important crystal modifiers on the surface of *n*-alkane wax crystal. An important paper in 2004, Molecular Physics studied the inhibitors of gas hydrate formation and wax depositons [9]. Gas hydrates are crystalline solids made of a host water lattice composed of cavities which enclathrate individual gas molecules [6]. The structure of the water lattice is determined by the size of the “guest” molecules and the composition of the gas mixture. Typical guest molecules include: methane, ethane, propane, carbon dioxide and hydrogen sulphide. Gas hydrate are formed when water and gas are together at low temperature and high pressure (e.g. temperature below 25 °C and pressures greater than 1.5 MPa for natural gas hydrate).

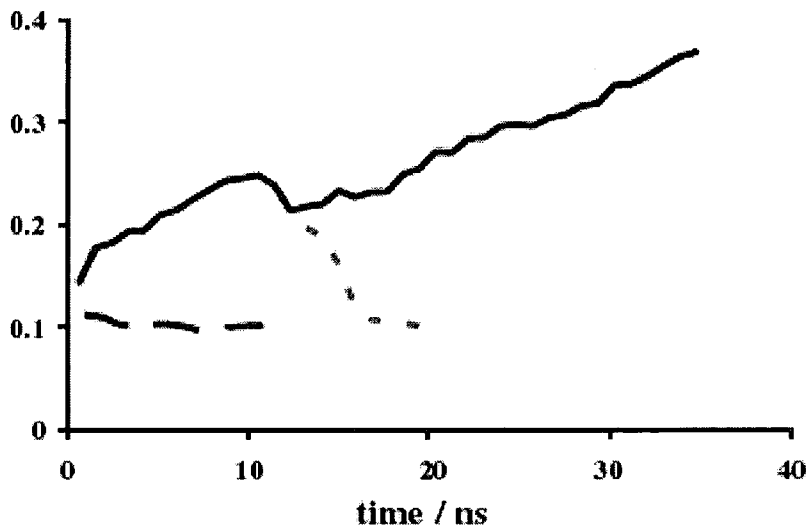
### 3.1 Molecular Simulation works using a kinetic inhibitors

In simulation work [9]- [10], a gas hydrate model can be made from a thin film of water surrounded by methane fluid.

To study inhibition, two model were used. In the first one a pure methane-water system (called uninhibited) was employed and compared to an equivalent system in which two octomers of polyvinylpyrrolidone (PVP) were added one at each water-methane interface.  $NpT$  Molecular Dynamics simulation was performed for both systems with the package DL\_POLY [11]. PVP was added by considering a configuration from the uninhibited simulation and putting the PVP within the methane fluid and close to the water surface. All water molecules were then immobilized and  $NVT$  MD were performed to relax any stress caused by the insertion. All simulations were carried out at  $T = 300$  K, which represents a subcooling of about 25 K respect to gas hydrate formation.

Results plotting the fraction of hydrate-like water molecules as a function of time for the uninhibited and inhibited simulation are shown in Figure 1.

Figure 1: Plot of the fraction of hydrate-like water molecules formed within time for an uninhibited (shown as solid line) and inhibited (shown as dashed lines) simulation (Figure 1 of ref. [10] used with permission).

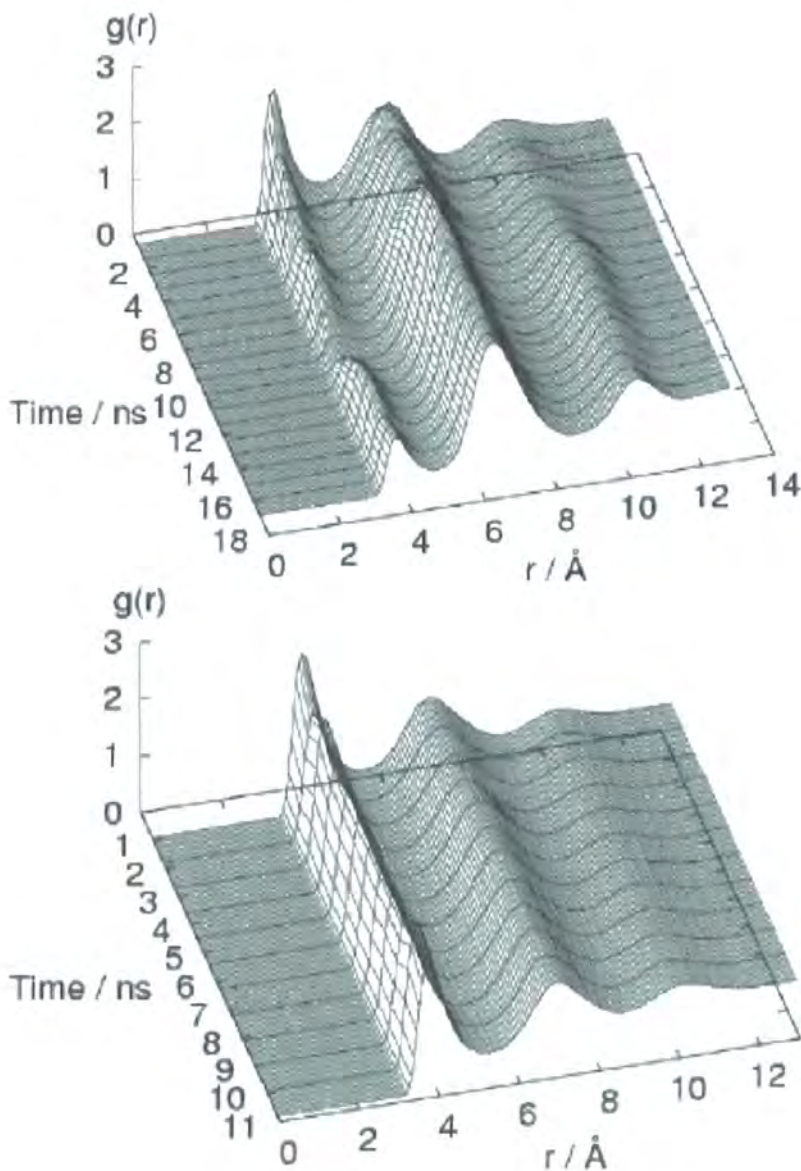


From Figure 1, after 35 ns more than one third of the water molecules are in

the hydrate phase. However, the introduction of PVP completely suppresses the growth. Hydrate clusters did not form when PVP was added at the beginning of the simulation, and PVP deformed the hydrate clusters when added after it had begun to form.

Radial distribution functions for the system water-methane system are shown in Figure 2.

Figure 2: Radial distribution function for the water-methane system in the uninhibited and inhibited simulation (Figure 2 of ref. [10] used with permission).



The RDFs in Figure 2 show three things.

- With time, the first peak disappears and the second peak shifts to about 7.5 Å; this indicate water-separated methane molecules.
- There is also a third peak at about 10 Å, showing long range ordering in the distribution of dissolved methane molecules.
- However, in the inhibited system there is no change of any peak with time, with no evident variation in either the height or position of the three peaks changing during more than 10 ns of the simulation when PVP was added at the beginning.

Is possible to conclude that direct simulation of methane hydrate is achievable with MD, and that the presence of PVP, as a kinetic inhibitor, increases the induction time for hydrate nucleation.

### 3.2 Molecular Simulation works using anti-agglomerants inhibitors

In 2000, Duffy and Rodger, described the effect of a particular anti-agglomerants inhibitors on paraffin crystal growth, using molecular dynamics calculation [10].

The interaction between an inhibitor, poly(octadecyl acrylate) (PA-18) and the low index face of a paraffin crystal ( $n$ -octacosane) was investigated using two different methods. The first involved collocating the inhibitor into the crystal with minimal disruption, by adding complete layers of crystal. The second one concerned rapid crystal growth by adding alkane molecules, one at a time, to a surface with an adsorbed PA-18 dimer.

The DL\_POLY software was used, and the united atom representation was employed for methylene and methyl group of the  $C_{28}H_{58}$  crystal.

The  $n$ -alkane crystal have a lamellar structure, with layers of molecules that are divided in blocks called lamellae, separated by well-defined gaps. The monoclinic structure of  $C_{28}H_{58}$  was used in those simulations; it has two molecules per unit cell and the molecular planes are stacked such that their short axes form a herring-bone configuration [12]. The (001) surface contains only the  $CH_3$  end groups arranged

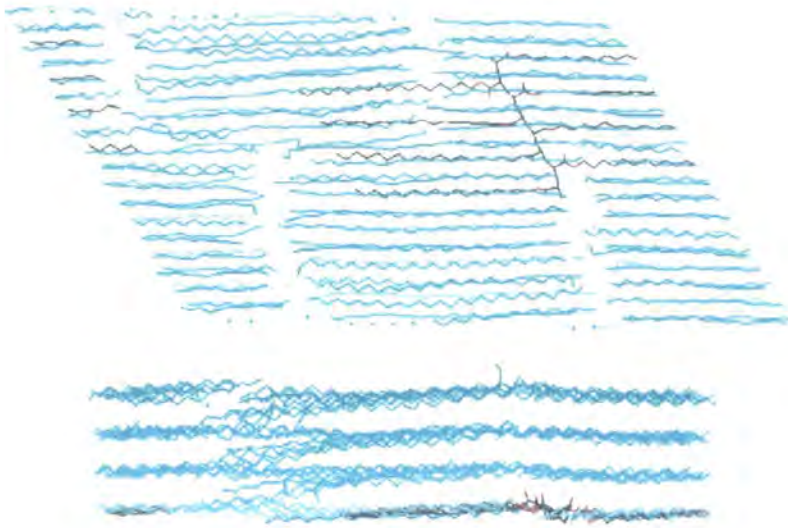
in a planar configuration; the (100) surface is corrugated and the surface molecules are widely separated. The (010) has the short axis of all molecules tilted at an angle to the plane of the surface, whereas the (110) surface has the short axes of the molecules oriented alternatively parallel and perpendicular to the surface plane.

Simulations of PA-18 on various surfaces of a *n*-octosane crystal have shown that PA-18 binds preferentially to the (110) and (010) surface. It was found that the PA-18 adsorb along the inter-lamellar gap, occupying the surface sites to which alkanes would have added if the crystal growth was uninhibited, as shown in Figure 3. When further layer of crystal wax were grown onto the inhibited surface it has been shown that these shifted so that the added alkanes lay over the inhibitor rather than aligning with the underlying crystal structure, as illustrated in Figure 4.

Figure 3: The PA-18 adsorbed on the (100) (shown on left) and (010) surface of an octosane wax crystal. Note that periodic boundary condition have been considered in order to show the inter-lamellar gaps across each surface (Figure 4 of ref. [10] used with permission).



Figure 4: Top and side view of a system in which three layers of crystal wax were added onto an inhibited surface (Figure 1 of ref. [10] used with permission) .



In summary have shown that PA-18 modifies the wax surface creating defects on it. At low concentration these defects prevent a step-growth mechanism.

## 4 Simulation Method for the Project

### 4.1 Force field models: molecular mechanics

#### 4.1.1 Introduction

This thesis will use typical molecular mechanic force fields to model diesel. The fact that force field approaches work is due to the validity of several assumptions:

- Nuclei and electron are lumped into atom-like particles.
- Atom-like particles are spherical and have a net charge.
- Interactions are based on springs (representing bonds) and classical potentials.
- Interactions must be pre-assigned to specific sets of atoms.
- Interactions determine the spatial distribution of atom-like particles and their energies.

The idea behind force field approaches are discussed below.

#### 4.1.2 The anatomy of a molecular mechanics force field

The approximation used for molecular mechanics calculations, as well as classical atomistic MD (molecular dynamic) and MC (Monte Carlo) simulation, is that the energy of a molecule can be describe as a function, termed a force field, that depends only on the atomic positions. This function, computes the molecular potential energy as a sum of terms that describe the variation of energy as a funtion of the deviation of bond lengths, bond angles and torsional angles away from equilibrium values, plus terms for non-bonded pairs of atoms describing Van der Waals and electrostatic interactions.

$$E = E_{\text{bonds}} + E_{\text{angle}} + E_{\text{dihedral}} + E_{\text{non-bonded}},$$

$$E_{\text{non-bonded}} = E_{\text{electrostatic}} + E_{\text{LJ}}. \quad (1)$$

There are many different force fields, which use different forms for the various interactions within and between molecules. The functional form of a force field depends on the accuracy required for its purpose. The common force fields in use today have been developed by using high-level quantum calculations and/or by fitting to experimental data.

A key property of all force fields is that a particular atom or group of atoms should have the same parameters in different molecules, i.e. they should be transferable. For example the stretching frequencies of aliphatic carbon-carbon bonds are largely independent of molecular environment, as are aliphatic C-H bonds lengths.

#### 4.1.3 Bond stretching

$E_{\text{bond}}$  is the energy function for stretching a bond between two atom types A and B. It is written as a Taylor expansion around an equilibrium bond length  $R_0$ . Terminating the expression at second order gives the following

$$E_{\text{bond}}(R^{AB} - R_0^{AB}) = E(0) + \frac{dE}{dR}(R^{AB} - R_0^{AB}) + \frac{1}{2} \frac{d^2E}{dR^2}(R^{AB} - R_0^{AB})^2. \quad (2)$$

The derivatives are evaluated at  $R = R_0$  and the  $E(0)$  term is normally set to zero; this is the zero point for the energy scale. The second term is zero because we consider the Taylor expansion around the equilibrium value. In its simple form the stretch energy can now be written as

$$E_{\text{bond}}(R^{AB} - R_0^{AB}) = K^{AB}(R^{AB} - R_0^{AB})^2 = K^{AB}(\Delta R^{AB})^2, \quad (3)$$

where  $K^{AB}$  is the force constant at  $R = R_0$  for the A-B bond. This is the form of a harmonic oscillator, the potential is quadratic in the displacement from the minimum.

The harmonic form is the simplest possible, and is in fact sufficient for determination of most equilibrium geometries. The reference bond length  $R_0$  is often called the equilibrium bond length. This is slightly misleading, as the reference bond length is the bond length when all the other force field terms are set to zero, while the actual equilibrium bond length is the bond length for the minimum energy configuration of the molecule.

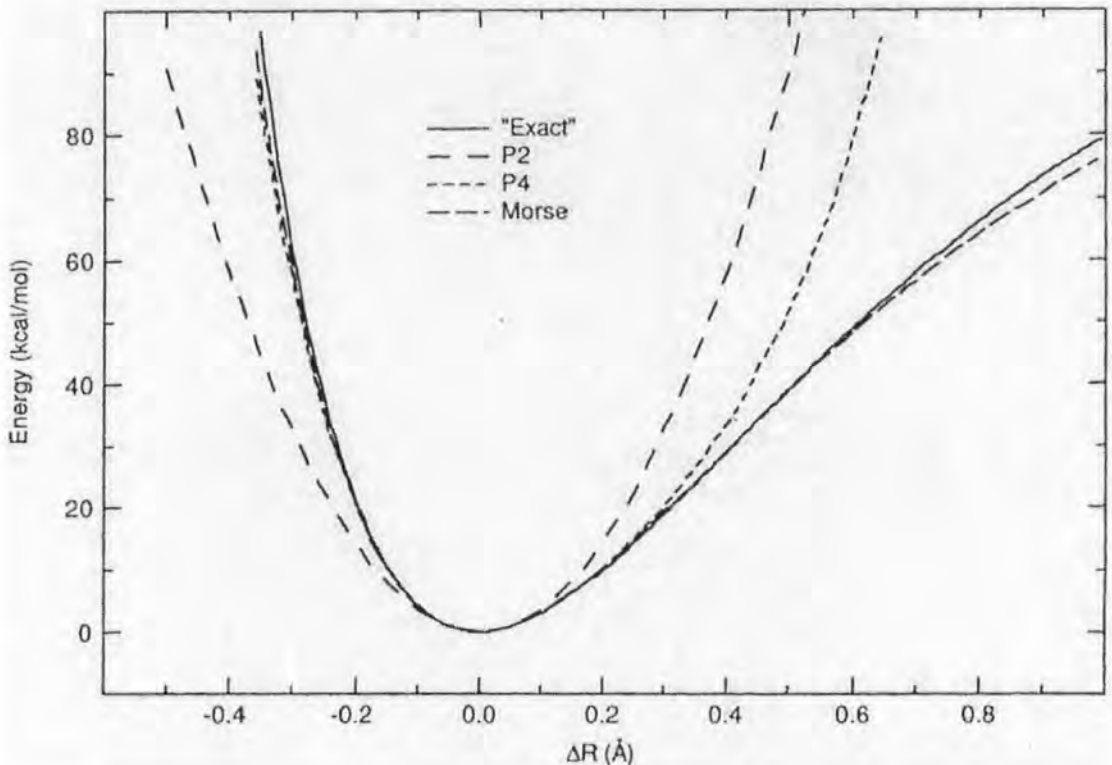
The forces between bonded atoms are very high in comparison to other forces. This is the justification for using the harmonic approximation (the harmonic oscillator). It is important to remember that this is an approximation to the real bond stretching potential and that for large deviations from  $R_0$  the harmonic approximation no longer holds true.

For situations where the bond lengths may deviate far from  $R_0$ , or to accurately calculate molecular structures and vibrational frequencies, it is necessary to go beyond the harmonic approximation and include higher order terms usually up to  $(R - R_0)^4$ . While increasing the range of validity of equation 3,  $E(R)$  will still tend to  $\infty$  as  $R \rightarrow \infty$ , so it remains unphysical. One potential, which satisfies the exact conditions outlined above, is the Morse potential [13]

$$E(R) = D(1 - \exp(-\alpha(R - R_0)))^2 \quad (4)$$

where  $D$  is the dissociation energy and  $\alpha = \sqrt{\frac{K}{2D}}$ .

Figure 5: Comparison of the performance of various functional forms for the stretch energy of CH bond in  $\text{CH}_4$ . The “exact curve “ is taken from an electronic structure calculation. (Figure taken from figure 2.1 of reference [14]).



The simple harmonic approximation (P2) in figure 5 is seen to be accurate to about  $0.1 \text{ \AA}$  from the equilibrium geometry and the quartic approximation (P4) up to  $0.3 \text{ \AA}$ . The Morse potential reproduces the real curve accurately up to an elongation of  $0.8 \text{ \AA}$ .

For the large majority of systems used in simulation, the only important chemical region is up to about  $10 \text{ kcal mol}^{-1}$  above the bottom of the curve. In this region a fourth order polynomial is essentially indistinguishable from either a Morse curve or the exact curve.

Values of the force constant are often evaluated from experimental data, such as infrared stretching frequencies, or from quantum mechanical calculations. Values

of bond length can be found from high-resolution crystal structures or microwave spectroscopy data.

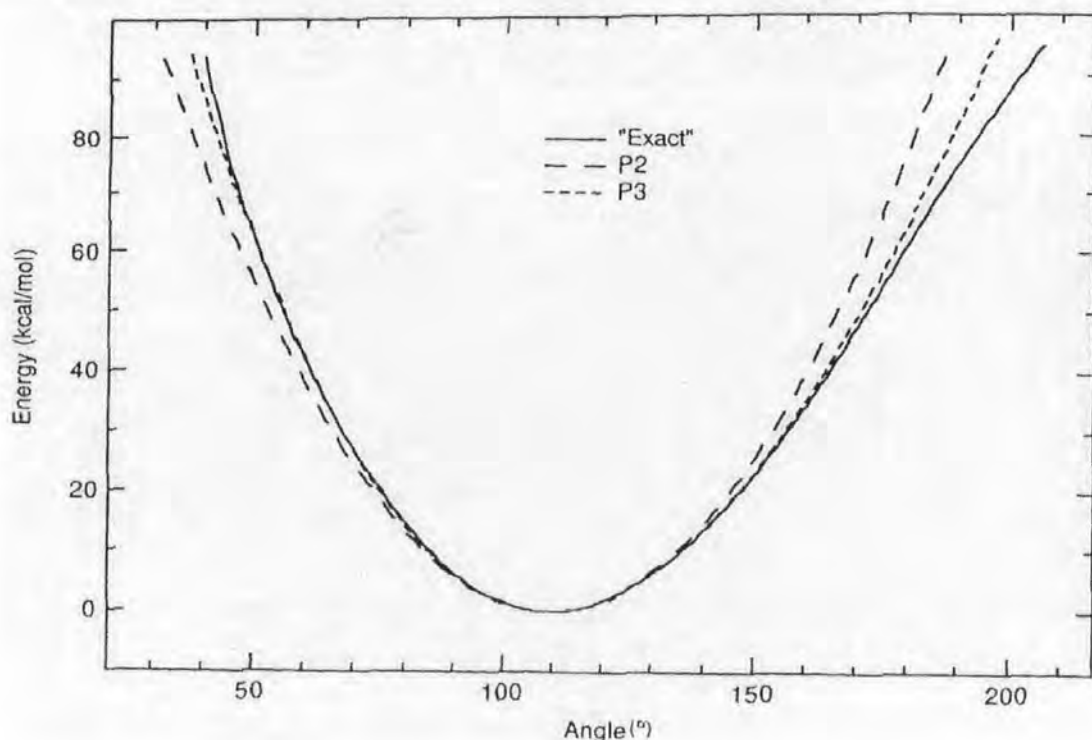
### Bond angle bending

$E_{\text{angle}}$  is the energy required for bending an angle formed by three atoms  $A-B-C$ , where there is a bond between  $A$  and  $B$ , and between  $B$  and  $C$ . In a similar way to  $E_{\text{bonds}}$  it is usually expanded as a Taylor series around a equilibrium bond angle and terminated at second order, giving the harmonic approximation:

$$E_{\text{angle}} (\theta^{ABC} - \theta_0^{ABC}) = K^{ABC} (\theta^{ABC} - \theta_0^{ABC})^2 . \quad (5)$$

While the simple harmonic expansion is quite adequate for most applications, there may be cases where higher accuracy could be useful. The next improvement is to include a third order term in the angle, as show in Figure 6 for  $\text{CH}_4$ .

Figure 6: Comparison of the performance of various functional forms for the angle bending energy of  $\text{CH}_4$ ; the “exact curve” form is taken from an electronic structure calculation. (Figure taken from Figure 2.4 of reference [14] )



The simple harmonic approximation (P2) is seen to be accurate to about  $\pm 30^\circ$

from the equilibrium geometry and the cubic approximation (P3) up to  $\pm 70^\circ$ .

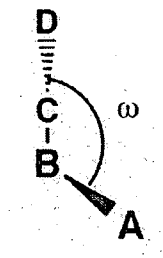
In the chemically important region below around  $10 \text{ kcal mol}^{-1}$  above the bottom of the curve, a second order expansion is analogous to  $E_{\text{bonds}}$ .

The energy needed to distort an angle away from equilibrium is much lower than the energy needed to distort a bond, so consequently bond angle bending forces tend to be proportionally smaller than those for bond stretching.

#### 4.1.4 Torsions

$E_{\text{dihedral}}$  is the energy change associated with rotation around a  $B - C$  bond in a four atom sequence  $A - B - C - D$ , where  $A - B$ ,  $B - C$  and  $C - D$  are bonded. Looking down the  $B - C$  bond, the dihedral (also called torsional) angle is defined as the angle formed by the  $A - B - C$  and  $D - C - B$  planes as illustrated in Figure 4.

Figure 7: Dihedral angle between the atoms  $A, B, C, D$ . (Figure taken from Figure 2.7 of reference [14]).



The torsional energy is different from  $E_{\text{bonds}}$  and  $E_{\text{angle}}$  in two aspects:

- First, the energy function must be periodic in the angle  $\omega$ : if the bond is rotated through  $360^\circ$  the energy should return to the same value.
- Second, the cost in energy for distorting a molecule by rotation around a bond is often low, i.e. large deviations from the minimum energy structure may occur.

A Taylor expansion in  $\omega$  is not a good idea, so in order to encompass the periodicity,  $E_{\text{dihedral}}$  is written as a Fourier series:

$$E_{\text{dihedral}}(\omega) = \sum_{n=1}^n V_n \cos(n\omega). \quad (6)$$

The term  $n = 1$  describes a rotation which is periodic by  $360^\circ$ , the  $n = 2$  term is periodic by  $180^\circ$ , the  $n = 3$  term is periodic by  $120^\circ$  and so on. The  $V_n$  constants determine the size of the barrier for rotation around the  $B - C$  bonds. Depending on the situation, some of the  $V_n$  constants may be zero. The form of  $E_{\text{dihedral}}$  is best understood by reference to an example. For ethane the most stable conformation is one where the hydrogens are staggered relative to each other, the eclipsed conformation represents an energy maximum. As the three hydrogens at each end are identical, there are three energetically equivalent staggered, and three equivalent eclipsed conformations. The rotational energy profile must have three minima and three maxima. In the Fourier series only those terms which have  $n = 3$  can have  $V_n$  constants different from zero.

Others terms could be necessary for rotation around single bonds in substituted systems. For example in the butane molecule, there are still three minima, but the two gauche (torsional angle  $\pm 60^\circ$ ) and anti (torsional angle  $= 180^\circ$ ) conformations now have different energies. The barriers separating the two gauche and the gauche and anti conformations are also of different height. So we have to introduce a term corresponding to  $n = 1$ .

For the ethylene molecule the rotation around the  $C = C$  bond must be periodic by  $180^\circ$ , and thus only  $n = 2, 4, \text{etc.}$  terms can enter.

In general molecules that are composed of atoms having a maximum valency of 4 (i.e. all the organic molecules), with a few exceptions are found to have rotational profiles showing at most three minima. The first three terms in the equation 6 are sufficient to qualitatively reproduce such a profile and combined with nonbonded interactions, can provide quantitative data.

Most rotational profiles resemble either the ethane or ethylene example above, and a popular expression for the torsion energy is

$$\begin{aligned}
E_{\text{dihedral}}(\omega^{ABCD}) &= \frac{1}{2}V_1^{ABCD} [1 + \cos(\omega^{ABCD})] + \frac{1}{2}V_2^{ABCD} [1 - \cos(2\omega^{ABCD})] \\
&+ \frac{1}{2}V_3^{ABCD} [1 + \cos(3\omega^{ABCD})].
\end{aligned}
\tag{7}$$

The + and - signs are chosen so that the one fold rotational term has a minimum for an angle of  $180^\circ$ , the two fold rotational term minima for angles of  $0^\circ$  and  $180^\circ$ , and the three fold term minima for angles of  $60^\circ$ ,  $180^\circ$  and  $300^\circ$  ( $-60^\circ$ ).

In simple form the three terms in the equation above can be described as:

$$E_1(\omega) = \frac{V_1}{2}(\cos \omega) \tag{8}$$

$$E_2(\omega) = \frac{V_2}{2}(\cos 2\omega) \tag{9}$$

$$E_3(\omega) = \frac{V_3}{2}(\cos 3\omega) \tag{10}$$

as illustrated in figure 8.

The total torsional energy is therefore given by

$$E_{\text{tot}}(\omega) = E_1(\omega) + E_2(\omega) + E_3(\omega) \tag{11}$$

as plotted in figure 9 .

Figure 8: The first three terms in a typical function to model the torsional energy.

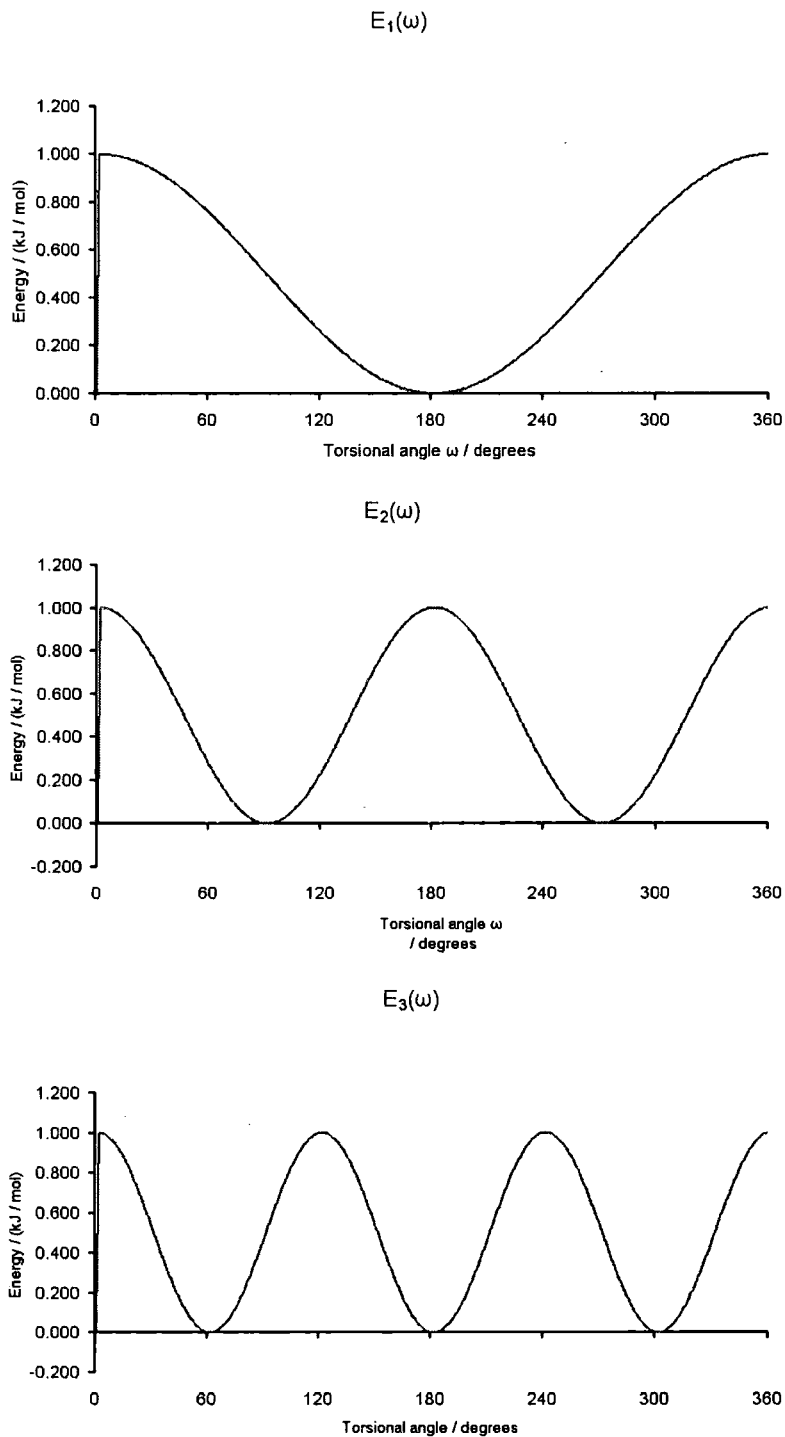
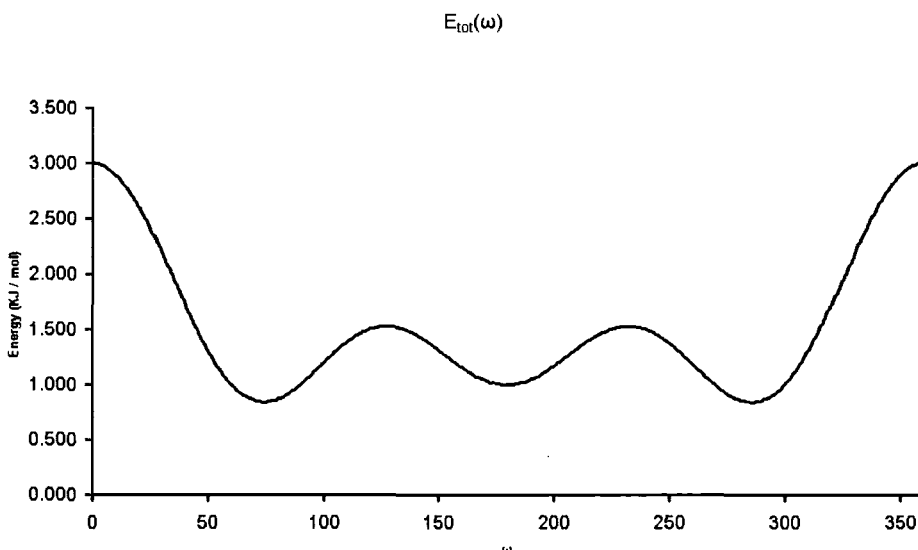


Figure 9: Total energy of torsion of a dihedral angle as a sum of the three terms in equation 11.



#### 4.1.5 Non bonded interactions

In addition to the bonded interactions between atoms described above, force fields also contain non-bonded interactions. Non-bonded interactions act between atoms in the same molecule and those in other molecules. Force fields usually divide non-bonded interactions into two: electrostatic interactions and Van der Waals interactions.

##### ELECTROSTATIC INTERACTIONS

The electrostatic interaction arises due to the unequal distribution of charge in a molecule. A simple example is the hydrogen fluoride (HF) molecule, where the hydrogen atom is slightly positive and the fluorine is slightly negative. Within the force field framework this uneven distribution of charge can be modeled by placing point charges at each of the atomic sites. Due to charge conservation for a neutral molecule these sum to zero. Thus in the previous example we would have  $q_F = -q_H$ . A Coulomb potential generally models the interaction between these point charges

$$E_{\text{elec}} = \frac{1}{4\pi\epsilon_0} \frac{q_i q_j}{r_{ij}}, \quad (12)$$

where  $\epsilon_0$  is the permittivity of free space,  $q_i$  are atomic charges, and  $r_{ij}$  is the distance between  $i$  and  $j$ .

#### VAN DER WAALS INTERACTIONS

$E_{\text{vdw}}$  is the van der Waals energy describing the repulsion and the attraction between atoms that are not directly bonded. At large interatomic distances  $E_{\text{vdw}}$  is zero and for small distances it becomes very repulsive. In quantum mechanical terms this is due to the overlap of the electron clouds of the two atoms: the electrons repel each other because they are negatively charged. At intermediate distance, there is a slight attraction between two such electron clouds. The attraction is due to induced dipole-induced dipole interactions (dispersion forces). Even if the molecule has not got a permanent dipole moment, the motion of electrons may create a slightly uneven distribution of charge at a given time. This transient dipole moment will induce a charge polarization in the neighboring molecule, creating an attraction.

It can be derived theoretically that this attraction varies, as a first approximation, as the inverse sixth power of the distance between the two fragments. The induced dipole-dipole interaction is only one of such terms: there are also contributions from quadrupole-dipole, quadrupole-quadrupole, etc. interactions. These vary as  $R^{-8}$ ,  $R^{-10}$ , etc.: the  $R^{-6}$  is only the asymptotic behavior at long distance.

$E_{\text{vdw}}$  is very positive at small distances, has a minimum, which is slightly negative at a distance corresponding to the two atoms touching each other, and goes towards zero faster as the distance become large.

A general functional form, which fits these considerations is :

$$E_{\text{vdw}}(R_{ij}^{AB}) = E_{\text{repulsive}}(R_{ij}^{AB}) - \frac{C_{ij}^{AB}}{(R_{ij}^{AB})^6}. \quad (13)$$

A popular potential, which obeys these general requirements, is the *Lennard-Jones* (LJ) potential [15], where the repulsive part is given by a  $R^{-12}$  dependence

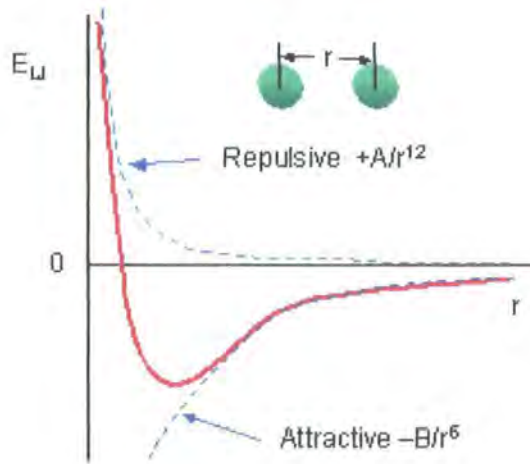
$$E_{\text{vdw}}^{LJ} = \frac{A_{ij}}{R_{ij}^{12}} - \frac{C_{ij}}{R_{ij}^6}, \quad (14)$$

where  $A_{ij}$  and  $C_{ij}$  are suitable constants.  $E_{\text{vdw}}$  can alternately be given as

$$E_{\text{vdw}}^{LJ} = 4\epsilon \left[ \left( \frac{\sigma_{ij}}{R_{ij}} \right)^{12} - \left( \frac{\sigma_{ij}}{R_{ij}} \right)^6 \right], \quad (15)$$

where  $\epsilon_{ij}$  is the Van der Waals well depth and  $\sigma_{ij}$  is the distance at which  $E_{\text{vdw}} = 0$ . The constants in equation 14 are related to  $\epsilon_{ij}$  and  $\sigma_{ij}$  by  $A_{ij} = 4\epsilon_{ij}\sigma_{ij}^{12}$  and  $C_{ij} = 4\epsilon_{ij}\sigma_{ij}^6$ .

Figure 10: Lennard-Jones Potential. (Figure taken from Chemistry Department Website of Saint Johns University, Minnesota, US).



There are no physical arguments for choosing the repulsive term to vary as  $R^{-12}$ ; this arises due to computational expediency. From electronic structure theory it is known that the repulsion is due to overlap of the electron wave function, and that the electron density falls off approximately exponentially with the distance from the nucleus (the exact wavefunction for an hydrogen atom is an exponential function). There is some justification for choosing the repulsive part as an exponential function.

The general form of the exponential  $R^{-6}$   $E_{\text{vdw}}$  function, also known as the "Buckingham" or "Hill" [16] type potential is

$$E_{\text{vdw}}^{\text{Hill}} = A_{ij} \exp(-B_{ij} R_{ij}) - \frac{C_{ij}}{R_{ij}^6} \quad (16)$$

where  $A_{ij}$ ,  $B_{ij}$  and  $C_{ij}$  are suitable constants.

#### 4.1.6 Different type of force field

##### CLASSICAL FORCE FIELDS:

- AMBER (Assisted Model Building and Energy Refinement) - widely used for proteins and DNA [17].
- CHARMM - originally developed at Harvard, widely used for both small molecules and macromolecules [18].
- CHARMM - commercial version of CHARMM, available through Accelrys.
- CVFF - also broadly used for small molecules and macromolecules.
- GROMOS - A force field that comes as part of the GROMOS (GRONingen Molecular Simulation package), a general-purpose molecular dynamics computer simulation package for the study of biomolecular systems. GROMOS force field (A-version) has been developed for application to aqueous or apolar solutions of proteins, nucleotides and sugars. However, a gas phase version (B- version) for simulation of isolated molecules is also available [19].
- OPLS-AA, OPLS-UA, OPLS-2001 - Members of the OPLS family of force fields developed by William L. Jorgensen at Yale Department of Chemistry [20].
- ECEPP/2 - free energy force field.

##### SECOND-GENERATION FORCE FIELDS:

- MMFF - developed at Merck, for a broad range of chemicals [21].
- MM2 [22], MM3 [23], MM4 [24] - developed by Norman L. Allinger, for a broad range of chemicals.

## 5 Molecular Dynamics Simulation

### 5.1 Introduction

Consider the energy of a state

$$E(M) = E(x, y, z, \dots, x_n, y_n, z_n). \quad (17)$$

Suppose we have a 2 state system with energies  $E_1$  and  $E_0$ . The relative populations of molecules in state 1 over state 0 is given by

$$\frac{N_0}{N_1} = \exp \left[ - \left( \frac{E_1 - E_0}{k_B T} \right) \right]. \quad (18)$$

If we have more than two states in a system it is possible to use the Boltzmann distribution to obtain the probability of each state. The probability of a state  $i$  is given by

$$P_i = \frac{\exp \frac{-(E_i - E_0)}{k_B T}}{q}, \quad (19)$$

where the quantity  $q$  is called the partition function.

The relation below gives the partition function  $q$

$$q = \sum_{i=1}^{N_{\text{states}}} \exp \left[ - \left( \frac{E_i - E_0}{k_B T} \right) \right] \quad (20)$$

where  $E_0$  is the lowest energy of the system and  $N_{\text{states}}$  is the number of different energy states.

This conditions is only useful for a small number of states. If we consider large molecules the number of conformations that are accessible is very large, too large to find all the relevant ones. If we have more than one molecule, the number of possible molecular arrangements grows exponentially as the number of molecules increases. It is impossible to solve this problem by calculating large number of energy states. Instead we need to calculate the average energies  $\langle E \rangle$ , without needing to calculate the partition function  $q$ .

Molecular dynamics (MD) allow us to “cheat” i.e. to calculate average quantities without considering the partition function  $q$ . We generate different states with the correct Boltzmann Distribution, so these states occur with a probability  $P_i$ . Consequently, the mean energy is given by an average over a representative number of states,

$$\langle E \rangle = \frac{\sum E_i}{\text{number of samples}}. \quad (21)$$

## 5.2 Molecular dynamic methods

### 5.2.1 Newton's Second Law

The molecular dynamics simulation method is based on Newton's second law

$$\mathbf{F}_i = m_i \mathbf{a}_i, \quad (22)$$

where  $\mathbf{F}_i$  is the force exerted on the particle  $i$ ,  $m$  is its mass and  $\mathbf{a}$  is its acceleration. From a knowledge of the force on each atom, it is possible to determine the acceleration of each atom in the system. Integration of the equations of motion then yields a trajectory that describes the positions, velocities and accelerations of the particles as they vary with time. From this trajectory, the average values of properties can be determined. The method is deterministic; once the positions and velocities of each atom are known, the state of the system can be predicted at any time in the future or the past. Molecular dynamics simulations can be time consuming and computationally expensive. However, computers are getting faster and cheaper. Simulations of solvated proteins can now be carried for tens of nanoseconds.

The force can also be expressed as the gradient of the potential energy (force field)

$$\mathbf{F} = - \nabla_i E_i. \quad (23)$$

Combining these two equations yields

$$-\frac{dE}{d\mathbf{r}_i} = m_i \frac{d^2 \mathbf{r}_i}{dt^2}, \quad (24)$$

where  $E$  is the potential energy of the system. Newton's equation of motion can then relate the derivative of the potential energy to the changes in position as a function of time. Solving these equations for a system of  $N$  atoms, means solving  $3N$  coupled  $2^{nd}$  order differential equations to yield the position vectors,  $\mathbf{r}_i$ , as a

function of time.

### 5.2.2 Integration algorithms

The potential energy is a function of the atomic positions ( $3N$ ) of all the atoms in the system. Due to the complicated nature of this function, there is no analytical solution to the equations of motion. Instead they must be solved numerically.

Numerous numerical algorithms have been developed for integrating the equations of motion mainly by using finite difference algorithms.

As examples we list:

- The Verlet algorithm [25] ;
- The Leap-frog algorithm [26].;
- The Velocity Verlet algorithm [26];
- The Beeman's algorithm [26].

In choosing which algorithm to use, one should consider the following criteria:

- The algorithm should conserve energy and momentum.
- It should be computationally efficient.
- It should permit a long time step for integration.

Most integration algorithms assume the positions, velocities and accelerations can be approximated by a form of Taylor series expansion.

#### THE VELOCITY VERLET ALGORITHM

▷ We start with  $\mathbf{r}(t)$ ,  $\mathbf{v}(t)$ ,  $\mathbf{a}(t)$ .

▷

$$\mathbf{r}(t + \delta t) = \mathbf{r}(t) + \mathbf{v}(t) \delta t + \frac{1}{2} \mathbf{a}(t) \delta t^2 \quad (25)$$

▷ Calculate the force

$$\mathbf{F} = - \nabla E(t + \delta t) \quad (26)$$

▷

$$\mathbf{F} = m\mathbf{a} \quad (27)$$

▷

$$\mathbf{a}(t + \delta t) = \frac{\mathbf{F}(t + \delta t)}{m} \quad (28)$$

▷

$$\mathbf{v}(t + \delta t) = \mathbf{v}(t) + \frac{1}{2} [\mathbf{a}(t) + \mathbf{a}(t + \delta t)] \delta t \quad (29)$$

▷ Now we have

$$\mathbf{r}(t + \delta t), \mathbf{v}(t + \delta t), \mathbf{a}(t + \delta t).$$

▷ Provide that  $dt$  is small, we can move forward in a series of steps. Iteration of these equations allows us to find  $\mathbf{r}$  as a function of time.

The leap-frog algorithm is also commonly used for molecular simulation and the details are discussed below.

#### THE LEAP-FROG ALGORITHM

$$\mathbf{r}(t + \delta t) = \mathbf{r}(t) + \mathbf{v}\left(t + \frac{1}{2}\delta t\right) \delta t \quad (30)$$

$$\mathbf{v}\left(t + \frac{1}{2}\delta t\right) = \mathbf{v}\left(t - \frac{1}{2}\delta t\right) + \mathbf{a}(t) \delta t \quad (31)$$

In this algorithm, the velocities are first calculated at time  $(\mathbf{v} + \frac{1}{2}\delta t)$ ; these are used to calculate the positions  $\mathbf{r}$ , at time  $(t + \delta t)$ . In this way, the velocities leap over the positions, and then the positions leap over the velocities. The advantage of this algorithm is that the velocities are explicitly calculated. The disadvantage is that they are not calculated at the same time as the positions. The velocities at time  $t$  can be approximated by the relationship

$$\mathbf{v}(t) = \frac{1}{2} \left[ \mathbf{v}\left(t - \frac{1}{2}\delta t\right) + \mathbf{v}\left(t + \frac{1}{2}\delta t\right) \right]. \quad (32)$$

The leap-frog algorithm can easily be applied to complex molecular systems and combined with constraint algorithms, such as the *SHAKE* procedure, which for example allows bonds lengths to be constrained, allowing longer time steps. Its

simplicity and speed makes it a useful choice for the work described in this study.

### 5.2.3 Statistical mechanics

In a molecular dynamics simulation, we study the macroscopic properties of a system through microscopic simulations. The connection between microscopic simulations and macroscopic properties is made via statistical mechanics [27], which provides mathematical expressions that relate macroscopic properties to the distribution and motion of the atoms and molecules of the  $N$ -body system.

The thermodynamic state of a system is usually defined by a small set of parameters: for example, the temperature  $T$ , the pressure  $p$  and the number of particles,  $N$ . Other thermodynamic properties may be derived from the equations of state and other fundamental thermodynamic equations.

The mechanical or microscopic state of a system is defined by the atomic positions,  $\mathbf{r}$  and momenta  $m\mathbf{v}$ ; these can also be considered as coordinates in a multi-dimensional space called phase space. For a system of  $N$  particles, this space has  $6N$  dimensions. A single point in phase space, describes the state of the system. An *ensemble* is a collection of points in phase space satisfying the conditions of a particular thermodynamic state. A molecular dynamics simulation generates a sequence of points in phase space as a function of time; these points belong to the same ensemble, and they correspond to the different configurations of the system and their respective momenta.

There exist different ensembles with different characteristics.

- *Micro canonical ensemble (NVE)*: The thermodynamic state is characterized by a fixed number of atoms,  $N$ , a fixed volume,  $V$ , and a fixed energy,  $E$ . This corresponds to an isolated system.
- *Canonical Ensemble (NVT)*: This is a collection of all systems whose thermodynamic state is characterized by a fixed number of atoms,  $N$ , a fixed volume,  $V$ , and a fixed temperature,  $T$ .
- *Isobaric-Isothermal Ensemble (NPT)*: This ensemble is characterized by a fixed number of atoms,  $N$ , a fixed pressure and a fixed temperature.

- *Grand canonical Ensemble* ( $\mu VT$ ): The thermodynamic state for this ensemble is characterized by a fixed chemical potential,  $\mu$ , a fixed volume,  $V$ , and a fixed temperature,  $T$ .

#### 5.2.4 Molecular dynamics and ensembles

Molecular dynamics [26] is most easily performed in the constant  $NVE$  ensemble. However, it is often of more interest to perform simulations in other ensembles such as the canonical and isobaric- isothermal ensembles.

##### MOLECULAR DYNAMICS AT CONSTANT TEMPERATURE ( $NVT$ ENSEMBLE)

As temperature is directly related to the average kinetic energies of all the particles in the system, and, from equipartition

$$K_E = \sum_{i=1}^N \frac{1}{2} m_i v_i^2. \quad (33)$$

The *Equipartition of energy* is a principle which states that, in a system in thermal equilibrium, on the average, an equal amount of energy will be associated with each independent energy state. Specifically, that for a system of particles in equilibrium at absolute temperature  $T$ ; each will have an average energy of  $\frac{1}{2} k_B T$  associated with each degree of freedom. For example, an atom of a gas has three degrees of freedom (the three spatial coordinates of the atom) and will, therefore, have an average total energy of  $\frac{3}{2} k_B T$ .

For  $N$  particles this will be

$$\frac{3}{2} N k_B T. \quad (34)$$

Now considering equation 33 and 34:

$$K_E = \sum_{i=1}^N \frac{1}{2} m_i v_i^2 = \frac{3}{2} N k_B T \quad (35)$$

and

$$T = \sum_i m_i v_i^2 / (3N k_B). \quad (36)$$

Constant temperature simulations can be carried out by scaling the velocity of

the particles. There are different types of thermostats for MD simulations in the literature [28]- [29], each one has advantages and disadvantages. All thermostats give a good temperature control, but they differ in how they drive the system to equilibrium. Some of most popular thermostats are described below.

The Anderson thermostat [28] keeps the temperature constant by colliding the particles with a heat bath. The strength of the coupling between the heat bath and the simulation can be determined by the frequency of stochastic collision,  $\omega$ , which can be selected by the simulator. During the simulation, particles are randomly selected and their velocities are set at values drawn from the Maxwell-Boltzmann distribution corresponding to the temperature of the heat bath.

In the thermostat proposed by N ose [30], the heat bath is represented by introducing an extra degree of freedom in the simulation. Energy can dynamically flow between the heat bath and the simulation system with a thermal inertia of  $Q$  ( $Q$  controls the thermal fluctuations in the system). Hoover simplified the approach by introducing a thermodynamic friction coefficient  $\xi$ .

The resulting N ose-Hoover thermostat equation of motion are:

$$\dot{\mathbf{r}}_i = \mathbf{p}_i/m_i, \quad (37)$$

$$\dot{\mathbf{p}}_i = \mathbf{f}_i - \xi \mathbf{p}_i, \quad (38)$$

$$\dot{\xi} = \frac{(\sum_i p_i^2/m_i - gk_B T)}{Q}, \quad (39)$$

where  $g$  is the number of degrees of freedom.

An alternative method for rescaling the velocity is the approach proposed by Berendsen [31]. At every time-step the old velocity  $\mathbf{v}$  are rescaled to new velocities,  $\mathbf{v}'$ , by  $\mathbf{v}' = \lambda \mathbf{v}$

$$\lambda = \left[ 1 + \frac{\Delta t}{\gamma} \left( \frac{T}{T_0} - 1 \right) \right]^{\frac{1}{2}}, \quad (40)$$

where  $T_0$  is the desired temperature and  $\Delta t$  is the integration time step.

Here,  $\gamma$  is the so-called “rise time” of the thermostat, describing the coupling strength of the system with a hypothetical heat bath. The larger the “rise time”, the weaker the coupling, i.e. the longer is the period of temperature fluctuations around  $T_0$ .

#### MOLECULAR DYNAMICS AT CONSTANT PRESSURE ( $NpT$ ENSEMBLE)

Ensemble that work in the constant pressure regime give the possibility to the simulation box of changing size during the course of the simulation. The box may be allowed to change isotropically or anisotropically depending on the method used and the system that is being studied.

In the Berendsen approach [31], the system is coupled to a pressure bath and obeys the equation:

$$\dot{p} = \frac{p_0 - p}{t_p}, \quad (41)$$

where  $p$  is the pressure of the system,  $p_0$  is the desired pressure, and  $t_p$  is a time constant. At each step the volume of the box is scaled by a factor of  $\xi$  and so the co-ordinates are scaled by a factor of  $\xi^{\frac{1}{3}}$  where

$$\xi = 1 - \lambda_T \frac{\delta t}{t_p} (p_0 - p), \quad (42)$$

and  $\lambda_T$  is a compressibility factor.

Nosé-Hoover barostat can also be used. In the form proposed by Toxvaerd [32] the co-ordinates  $Q^N$  are scaled to  $R^N = Q^N V^{\frac{1}{3}}$ . Introducing a friction,  $\xi$ , the equations of motion become:

$$\dot{\mathbf{r}} = \frac{\mathbf{P}_i}{(m_i V^{\frac{1}{3}})}, \quad (43)$$

$$\dot{\mathbf{p}}_i = \mathbf{f}_i - (\dot{\xi} + \xi) \mathbf{p}_i, \quad (44)$$

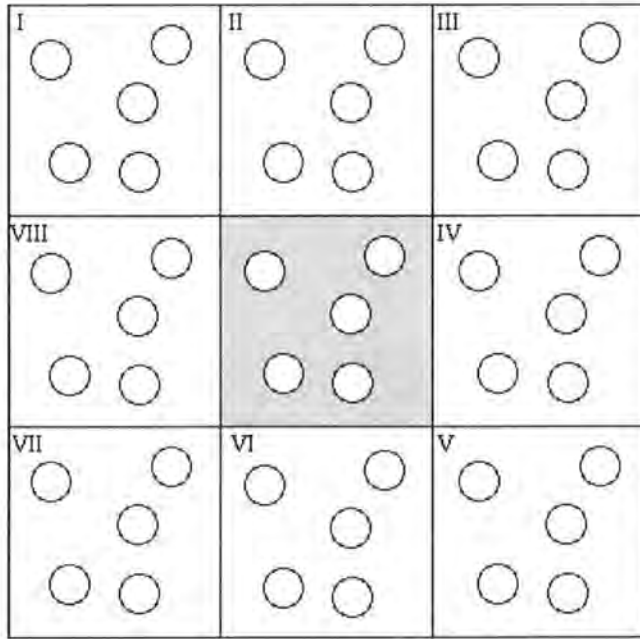
$$\dot{\xi} = \frac{V \cdot}{(3V)}, \quad (45)$$

$$\ddot{\xi} = \frac{(P - P_0)V}{Nk_B T t_p^2}, \quad (46)$$

where  $\dot{\xi}$  is given by equation 39.

#### PERIODIC BOUNDARY CONDITIONS

Figure 11: Periodic boundary condition. (Figure taken from Figure 2.4 of reference [14]).



Periodic boundary conditions enable a simulation to be performed using a relatively small number of particles in such a way that the particles experience forces as though they were in a bulk solution. See, for example, the two dimensional box shown in Figure 11. The central box is surrounded by eight neighbours. The coordinates of the image particles, those found in the surrounding box, are related to those in the primary box by simple translations. The simplest box is the cubic box. Forces on the primary particles are calculated from particles within the same box as well as in the image boxes (nearest image conversion). The cutoff is chosen such that a particle in the primary box does not see its image in the surrounding boxes.

## 6 Assessment of force field for hydrocarbons

In this project we are studying hydrocarbons and in particular  $n$ -linear and branched alkanes.  $n$ -alkanes are nonpolar, flexible chain molecules. They are composed of only two types of segment, methyl and methylene groups.  $n$ -alkanes are used as feedstock for the production of natural gas, petrochemicals, gasoline, kerosene, oil, paraffin wax and are one of the building blocks for biological molecules (e.g. phospholipids).

In the literature two different approaches for dividing alkanes into interaction sites are followed when building a transferable molecular force field. The term *transferable* is the key word for the force field; it implies that the force field parameters for a given interaction site should be transferable between different molecules (e.g. identical parameters should be used for the methyl group in, say,  $n$ -hexane, 1-hexene, or 1-hexanol) and that the force field should be transferable to different state points (e.g., pressure, temperature, or composition) and to different properties (e.g., thermodynamic, structural, or transport).

The first approach is to consider each hydrogen and carbon atoms as an interaction site, and is called an "ALL-ATOM FORCE FIELD". The second approach is to unite each carbon and its bound hydrogen into a single interaction site, to give a "UNITED-ATOM FORCE FIELD".

In the united-atom approach, according to the above consideration, the number of interaction sites is reduced by a factor of approximately three and thus the computational burden is reduced by an order of magnitude ( $2n^2$ ). The choice of simulation can change drastically when we choose one method or the other. It depends which type of molecules we want to study. In the simulation of  $n$ -alkanes where the number of hydrogens is very high, using a "united-atom" force field make our simulation easier but with some loss in accuracy. However, a literature search reveals several united atom studies for hydrocarbons, which have succeeded in producing excellent agreement with experimental data. In the following paragraph, we briefly summarise the best known and useful types of force field and the conclusions we have made.

## 6.1 Different force field for hydrocarbons

Three literature force fields for hydrocarbons are considered below: *OPLS-UA*, *TraPPE* and *NERD*

### 6.1.1 OPLS-UA

The united atom form of the OPLS (Optimised Parameters for Liquid Simulation) force field was developed by in Jorgensen’s laboratory at Yale University, Chemistry Department from the 1978 to 1984.

In reference [33] optimized intermolecular potential functions have been determined for hydrocarbons through Monte Carlo simulations of different liquids. To achieve high accuracy, 12 unique group types were identified and their associated Lennard-Jones parameters were established. The average deviation from experiment for the computed densities and heats of vaporization was 2%.

The functional form for the bonding interactions, harmonic bond stretching and bending is seen in equation 3, 5 and the parameters for the force field are summarised in Table 6, 4, 5. In common with many united atom force fields, Jorgensen chose to freeze bond lengths at their equilibrium values, which is justified based on the fact that bond lengths only change a little from equilibrium values and the coupling between bond stretching and bond bending is weak.

Table 1: Lennard Jones 12-6 parameters for OPLS-UA force field.

Atom Type	$\epsilon/\text{kcal mol}^{-1}$	$\sigma/\text{\AA}$	$q/e^-$
C2-C2	0.1180	3.905	0.00
C3-C3	0.1750	3.905	0.00
C2-C3	0.1437	3.905	0.00

Table 2: 1-2 Interaction [Stretch] for OPLS-UA force field.

Atom Type	Bond lengths / Å
C4-C4	1.53
C4-C3	1.50
C3=C3	1.34
C3-C3	1.40

Table 3: 1-3 Interaction [Bend] for OPLS-UA force field.

Bend Type	Bond angles / deg	$(K_\theta/k_B)/\text{K}$
C-C4-C	112	62,500.00
C-C3-C	124	62,500.00

The torsional angles are generated according to the torsional potential

$$\begin{aligned}
 E_{dihedral}(\omega^{ABCD}) &= \frac{1}{2}V_1^{ABCD} [1 + \cos(\omega^{ABCD})] + \frac{1}{2}V_2^{ABCD} [1 - \cos(2\omega^{ABCD})] \\
 &+ \frac{1}{2}V_3^{ABCD} [1 + \cos(3\omega^{ABCD})]
 \end{aligned}
 \tag{47}$$

with  $V_1 = 1.411 \text{ kcal mol}^{-1}$ ,  $V_2 = -0.271 \text{ kcal mol}^{-1}$ ,  $V_3 = 3.145 \text{ kcal mol}^{-1}$ .

### 6.1.2 TraPPE (Transferable Potential for Phase Equilibria Force Field)

This force field was developed by the research group of Siepmann of the University of Minnesota, Chemistry Department [33]- [34].

Table 4: 1-2 Interaction [Stretch].

Stretch Type	Distance / Å
CHx-CHy	1.540

Table 5: 1-3 Interaction [Bend].

Bend Type	$\theta$	$(K_\theta/k_B)/K$
CHx-(CH)-CHy	112.0	62,500.00

Table 6: Lennard Jones 12-6 parameters.

Atom Type	$(\epsilon/k_B) / K$	$\sigma / \text{\AA}$	$q / e^-$
[CH3]-CHx	98.00	3.75	0.00
[CH]-(CH3)3	10.00	4.68	0.00
CHx-[CH2]-CHy	46.00	3.95	0.00

The torsional angles are generated according to the torsional potential

$$\begin{aligned}
 E_{dihedral}(\omega^{ABCD}) &= \frac{1}{2}V_1^{ABCD} [1 + \cos(\omega^{ABCD})] + \frac{1}{2}V_2^{ABCD} [1 - \cos(2\omega^{ABCD})] \\
 &+ \frac{1}{2}V_3^{ABCD} [1 + \cos(3\omega^{ABCD})]
 \end{aligned}
 \tag{48}$$

with  $V_1 = 1.411 \text{ kcal mol}^{-1}$ ,  $V_2 = -0.271 \text{ kcal mol}^{-1}$ ,  $V_3 = 3.145 \text{ kcal mol}^{-1}$ .

In order to optimise these parameters the Siepmann group have worked extensively on  $n$ -alkanes over many years employing the technique of Gibbs ensemble Monte Carlo combined with the configurational-bias Monte Carlo method to determine the vapour-liquid curves of various  $n$ -alkanes. Different alkanes models have been compared and the model parameters have been optimised to describe the vapour-liquid curve over a large temperature range [35]. Siepmann demonstrated that for modelling vapour liquid coexistence a relatively simple united-atom model is sufficient to obtain a very good agreement with experimental data and it is not necessary to take the hydrogen atoms explicitly into account. Also, in contrast with the traditional view, the critical density of the long alkanes decreases rather than increases with carbon numbers.

### 6.1.3 NERD

The NERD force field was introduced to model branched and linear alkanes. Monte Carlo simulations have been conducted to assess the ability of this force field to predict orthobaric density, second virial coefficients, and  $p - V - T$  data for short and long alkanes [36]. The force field provides good agreement with experimental phase equilibrium and second virial coefficient data over wide ranges of temperature. In another article the NERD force field has been used to study the vapour-liquid equilibria for pure components and binary mixtures [37]. Result of phase equilibria simulations are found to be in good agreement with available experimental data. The force field has also been used to study vapour-liquid equilibria for various isomers of alkanes up to  $C_8$ . Results from this simulation are found to be in quite good agreement with experimental data [38]. In the NERD force field the bonding parameters are the same as in TraPPE. However, the Lennard-Jones parameters change slightly as shown in table 7.

Table 7: Non-bond interaction in TraPPE and NERD force field.

	TraPPE	NERD
CH2 ( $\epsilon/k_B$ )/K	46.0	45.8
CH3( $\epsilon/k_B$ )/K	98.0	140.0
CH2 $\sigma/\text{\AA}$	3.95	3.93
CH3 $\sigma/\text{\AA}$	3.75	3.91

## 6.2 A comparison of force field for $n$ -hexane.

To compare the above force field, molecular dynamics simulations of  $n$ -hexane were carried out using the DL POLY simulation program, version 2.13.

DL POLY is a general purpose serial and parallel molecular dynamics simulation package originally developed at Daresbury Laboratory, Cheshire, UK by W. Smith and T.R. Forester. Any molecular dynamic simulation performs five different kinds of operations:

- Initialisation,

- Force calculation,
- Integration of the equation of motion, Newton's second law.
- Calculations of system properties
- Job termination.

In order to perform these processes DL POLY required three *input data files*.

- CONTROL, tells the program which kind of simulation we want to run, how many data we want to gather and for how long the job running. These essential parameters such as temperature, pressure, number of steps required, simulation algorithm, ensemble used, the job time and the close time.
- CONFIG, contains all the coordinates of the atoms in the simulation.
- FIELD, specifies the nature of the inter- and intramolecular interactions, the molecular topology and the atomic properties like charge and atomic mass.

A successful run of DL POLY will generate several data file, which appear in the executive sub directory, called *output data files*. This data file contains a summary of the simulation: the input information, the starting configuration, temperature, pressure, timestep, etc. (all the data from the CONTROL file), thermodynamic data, the final configuration and radial distribution functions.

- REVIVE, is a binary file, used as input to allow a simulation to be restarted.
- REVCON, this has the same format as a CONFIG file and can be used to restart a simulation from the final configuration of an old simulation.
- STATIS, summary of instantaneous values of thermodynamic and other variables, in a form suitable for statistical analysis.
- HISTORY, provides time ordered sequence of configurations to facilitate further analysis of atomistic motion.

### 6.2.1 The steps required in a MD simulation using hexane as an example

To compare hexane in the OPLS-UA, TraPPE and NERD force fields we carried out molecular dynamics simulations for a small system of 216 *n*-hexane molecules in a cubic simulation box. The following steps were used:

- The molecular structure of *n*-hexane was produced in a modelling program (Maestro) to generate initial coordinates.
- Coordinates for many molecules were generated, making a lattice of molecules through a FORTRAN program and generating coordinates by duplications of the single molecule. e.g. for a 6\*6\*6 lattice in a cubic simulation cell, 216 molecules are created (1080 atoms).
- FIELD file with the force parameters for OPLS-UA, TraPPE, or NERD was created.
- CONTROL file was created.
- DL POLY was run for 100,000 steps in the *NVT* ensemble in order to melt the lattice and have a gas phase, at room temperature (298 K), using the leap frog algorithm. A time step of 2 fs was employed and the SHAKE algorithm was used to constrain bond lengths to equilibrium values.
- DL POLY was run for 1,000,000 steps in the *NpT* ensemble using the Berendsen thermostat and barostat and a high pressure of 1000 atm, to rapidly compress to a liquid phase. Temperature and pressure relaxation times of 1 ps and 4 ps respectively was used.
- DL POLY was run for 1,000,000 steps in the *NpT* ensemble using the Berendsen thermostat and barostat in order to have liquid phase; at room temperature (298 K) and a pressure of 1 atm.
- DL POLY was run for 1,000,000 steps in the *NpT* ensemble using Nosé-Hoover thermostat and barostat in order to have an equilibrated liquid phase; at room temperature (298 K) and a pressure of 1 atm. As before employing temperature and pressure relaxation times of 1 ps and 4 ps respectively.

### 6.2.2 Result

We give below results from three force fields for simulations of 216 *n*-hexane molecules; and assess them with a view to choosing a force field for future simulations.

#### OPLS-UA

Average density calculated:  $0.6808 \text{ g cm}^{-3}$ ; experimental density:  $0.6603 \text{ g cm}^{-3}$ .

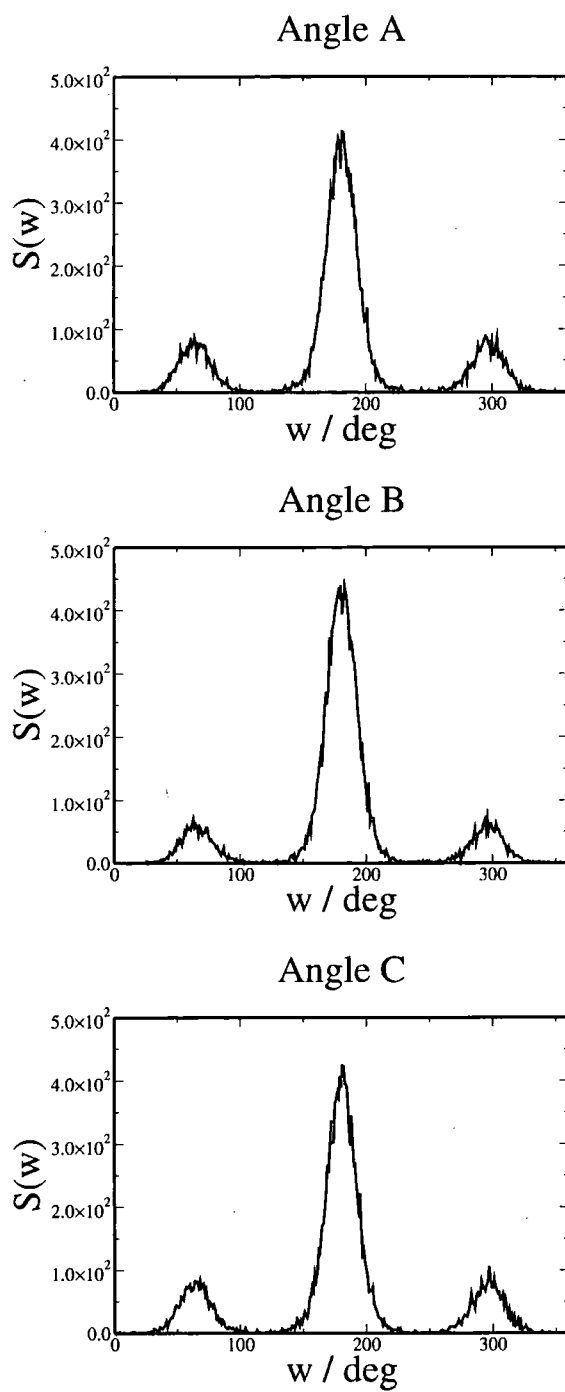
An important property in order to evaluate from molecular simulation is the dihedral angle distribution function. In hexane we have three dihedral angles, that we call angle A (formed by the atoms 1,2,3,4), angle B (formed by the atoms 2,3,4,5), angle C (angle formed by the atoms 3,4,5,6). The distribution function,  $S(w)$ , for these three are shown in Figure 12.

The result in the Figure and Table above are in excellent agreement with previous simulation results [36] and experimental Raman scattering data where a trans population of 70.7 % is given [39]- [40] for angle A.

Table 8: % trans-gauche populations of the three dihedral angles in hexane using the OPLS-UA force field.

	Angle A	Angle B	Angle C
Gauche + (%)	14.79166	11.1458	14.6875
Trans (%)	70.4456	77.67939	70.3067
Gauche - (%)	14.7627	11.1747	15.00579

Figure 12: Dihedral angle distribution functions for angles A-C using the OPLS-UA force field.



## NERD

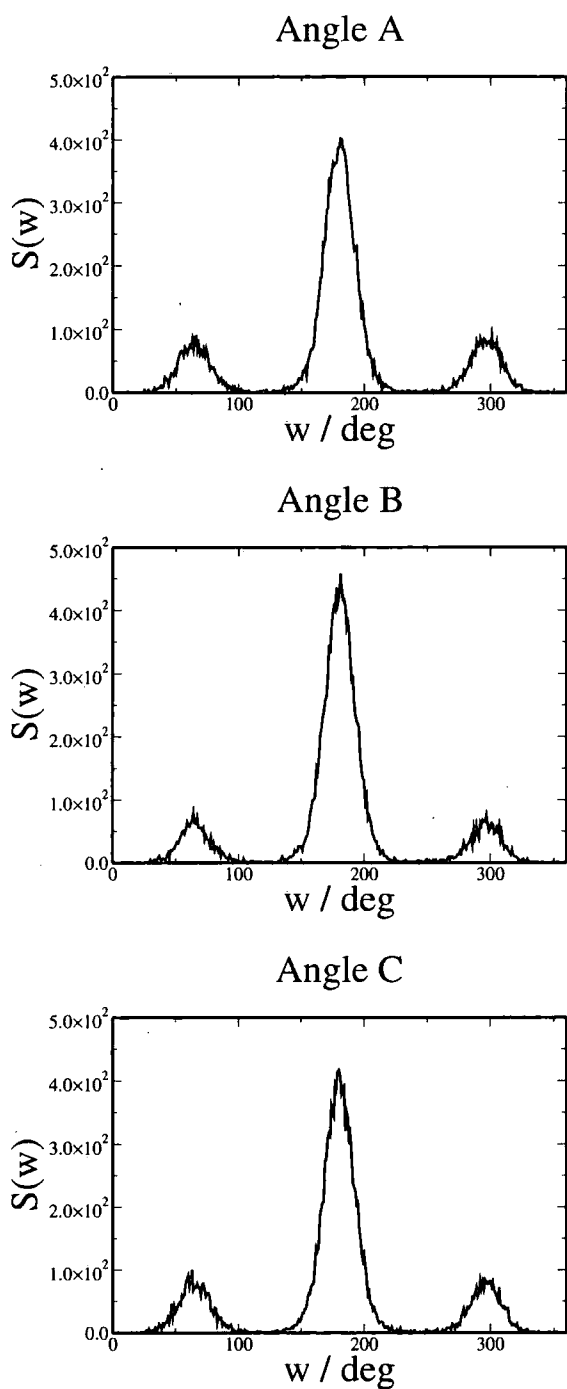
Average density calculated:  $0.6479 \text{ g cm}^{-3}$  ; experimental density:  $0.6603 \text{ g cm}^{-3}$  .

The dihedral angle distributions given using the NERD force field are show in figure 13.

Table 9: % trans-gauche populations of the three dihedral angles in hexane using the NERD force field.

	Angle A	Angle B	Angle C
Gauche + (%)	14.73379	11.42631	15.0690
Trans (%)	69.94210	76.96759	70.6134
Gauche - (%)	15.32407	11.60880	14.3171

Figure 13: Dihedral angle distribution functions in hexane for angles A-C using the NERD force field.



The result in the figure and in the table above are also in agreement with previous simulation [36], and experimental Raman scattering data where a trans population of 70.7 % is given [39]- [40] for angle A.

## TRAPPE

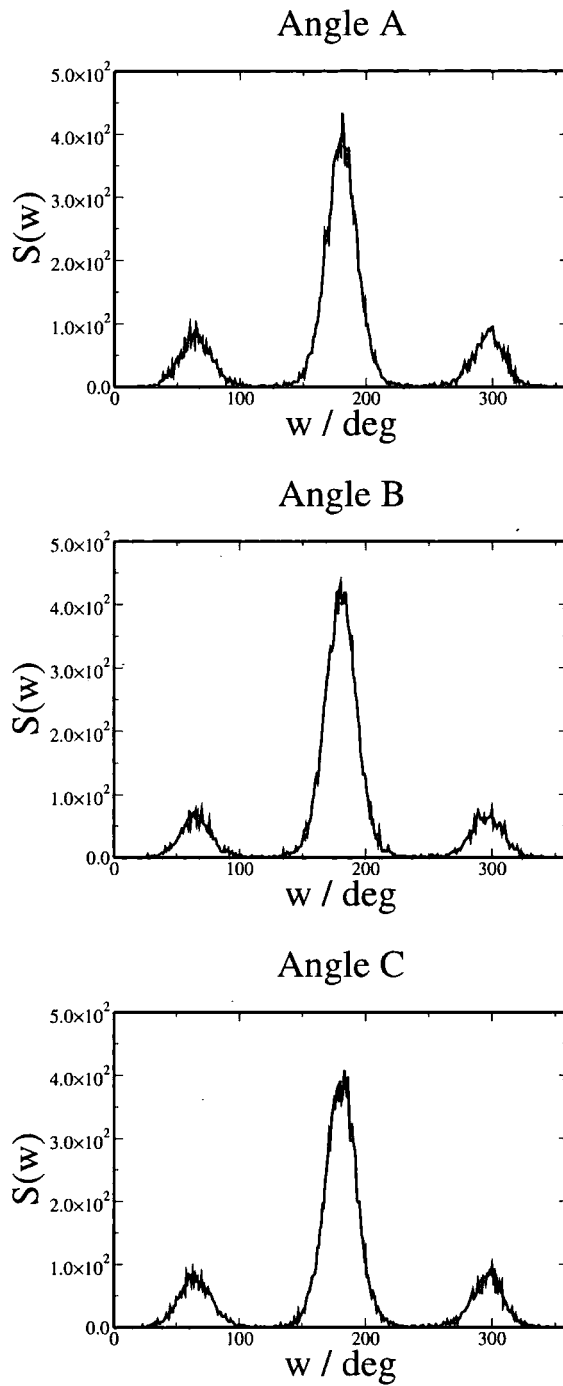
Average density calculated:  $0.6679 \text{ g cm}^{-3}$  ; experimental density:  $0.6603 \text{ g cm}^{-3}$  .

The dihedral angle distribution given using TraPPE force field are show in figure 14.

Table 10: % Trans-gauche population of the three dihedral angles in hexane using the TraPPE force field.

	Angle A	Angle B	Angle C
Gauche + (%)	15.1331	11.8630	15.0221
Trans (%)	69.6060	75.5840	70.2310
Gauche - (%)	15.2600	11.5520	14.7430

Figure 14: Dihedral angle distribution functions for angles A-C using the TraPPE force field



The results are also in excellent agreement with previous simulation [36] and experimental Raman scattering data where a trans population of 70.7 % is given [39]-[40] for angle A.

The results for the three force fields are all very similar. The TraPPE-UA gives slightly better agreement with experiment, with slightly better values for the trans/gauche distribution. Moreover, this force field has an advantage over NERD, in so much as there are a whole set of parameters available for other non-hydrocarbons. It makes sense therefore to choose this force field for further simulations.

### 6.3 Accurate description of TraPPE-UA force field

As discussed in the previous chapter the TraPPE-UA force field was chosen. Before discussing diesel simulations, a brief but more accurate description of this force field is appropriate.

For this project, the simplest and easiest to simulate force field, TraPPE-UA is the most useful. This force field utilizes pseudo-atoms located at carbon centres for alkyl groups (CH<sub>4</sub>, CH<sub>3</sub>, CH<sub>2</sub>, CH, and C). The total potential energy is divided into a bonded and a non bonded part. The non bonded potentials are used only for the interactions of pseudo-atoms belonging to different molecules or belonging to the same molecule but not accounted for by any of the intramolecular bonded potentials. The intramolecular bonded potentials include: fixed bond lengths for neighbouring pseudo-atoms (1-2 interactions), harmonic bond bending potentials for pseudo-atoms separated by two bonds (1-3 interactions), and dihedral potentials for pseudo-atoms separated by three bonds (1-4 interactions) and thus takes an almost identical functional form to the OPLS force field.

The potential function for the TraPPE force field is as follow [33]- [34]:

$$\begin{aligned}
 E(r_N, q_N) &= \sum_{i < j} \left( \frac{q_i q_j}{4\pi\epsilon_0 r_{ij}} \right) + \sum_{i < j} u(r_{ij}, q_i, q_j) \\
 &+ \sum_{\text{dihedral}} u_{\text{dih}}(\phi) \\
 &+ \sum_{\text{angles}} \frac{k_\theta}{2} (\theta - \theta_{eq})^2 + \sum_{\text{bonds}} \frac{k_l}{2} (l - l_{eq})^2
 \end{aligned} \tag{49}$$

where  $r_N$ ,  $q_N$ ,  $r_{ij}$ ,  $\theta$ ,  $\phi$ , and  $l$  are the set of Cartesian coordinates and partial

charges, the pair separations, bending angles, the dihedral angles and the bond lengths respectively.

## 7 Simulation of a model diesel

A simulation containing 78.7 % of a branched solvent (2,4,6,10 tetramethyl dodecane) plus a distribution of *n*-alkanes from C<sub>10</sub> up to C<sub>26</sub> was studied.

The component of each *n*-alkane in a typical diesel are shown in table 11 and in figure 15. A cut off of C<sub>26</sub> was applied to the model system because above C<sub>26</sub> the percentage of higher alkanes in the mixture is very low. The % of *n*-alkanes employed in our model diesel is given in table 12.

Figure 15: The distribution of *n*-alkanes in a typical diesel up to C<sub>26</sub>. Data is supplied by Infineum.

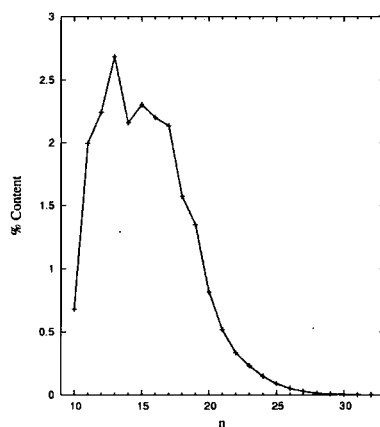


Table 11: % of linear saturated hydrocarbons in a typical diesel fuel. Data is supplied by Infineum.

C	% In Fuel
10	0.680
11	1.996
12	2.243
13	2.683
14	2.159
15	2.304
16	2.199
17	2.135
18	1.574
19	1.346
20	0.815
21	0.518
22	0.334
23	0.231
24	0.148
25	0.090
26	0.051

Table 12: % of linear saturated hydrocarbons in our model diesel

C	% in our model diesel
10	0.680
11	1.996
12	2.243
13	2.683
14	2.159
15	2.304
16	2.199
17	2.135
18	1.574
19	1.346
20	0.815
21	0.518
22	0.334
23	0.231
24	0.148

The steps required for setting up this model diesel simulation are:

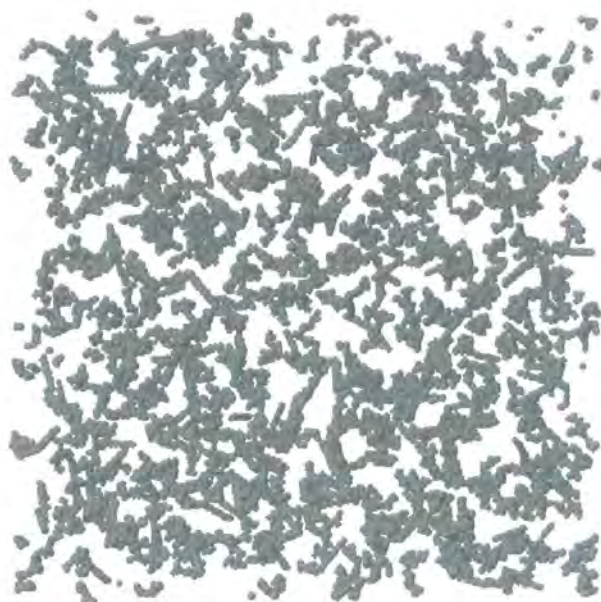
- Draw the single molecules of the distribution and the solvent with a molecular modeling program (Maestro), which provides a pdb file, containing the cartesian coordinates and the connectivities of the atoms.
- Create coordinates for many molecules, making a low density lattice of the mixture using a Fortran program and generating coordinates by duplications of the single molecules.
- Create a DL\_POLY FIELD file using a Fortran program to assign TraPPE force field parameters to structural features of each molecule.
- Create a CONTROL file to control the simulation.
- Run the molecular dynamics program, DL\_POLY, for 1,000,000 steps in the  $NpT$  ensemble using the Berendsen thermostat and barostat and a high pressure of 1 Katm, in order to compress the diesel mixture from a lattice to a liquid phase, at room temperature (298 K), using a leap frog algorithm. (Employ a time step of 2 fs and the SHAKE algorithm to constrain bond lengths to equilibrium values).
- Further compression, as described in table 13 and discussed below.
- Equilibrate the mixture at 1 atm of pressure at room temperature (298K) using a Nosé-Hoover thermostat and barostat.

Initial simulations lead to condensation of liquid droplets within the gas phase, leading to a highly inhomogeneous system. This is illustrated in the snapshot from figure 16, which show large gaps between molecules. This caused major problems in equilibration during standard molecular dynamics runs.

After approximately 3 weeks of computer time, with large cutoff parameters, the model diesel looked much better as show in figure 17.

The actual liquid diesel density is  $0.83 \text{ g cm}^{-3}$ .<sup>1,2</sup>

Figure 16: Snapshot of the model diesel compressed from gas phase towards a liquid, where the molecules have condensed into clusters of diesel liquid leaving gaps between the cluster.

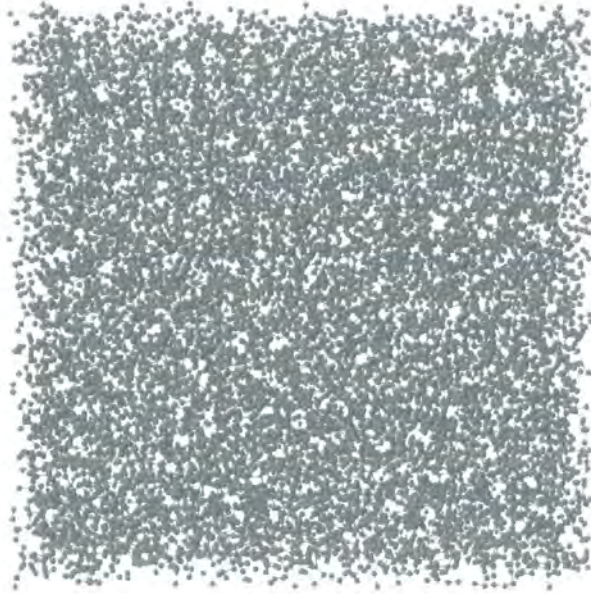


---

<sup>1</sup>Initial simulation crashed due to certain molecules being too close and therefore generating large repulsion forces. Starting the simulation again with an expanded box, solved the first error, but an other error was found. The problem was that the Neighbour list arrays employed by the DL\_POLY program are too small. This means that the construction of the Verlet neighbour list (in subroutine *link\_cell\_pairs*) failed because the number of non-bonded pair exceeded the neighbourlist array dimension. This problem arises when there are inhomogeneties in the density within a simulation box.

<sup>2</sup>This problem can be solved by modifying two parameters in the CONTROL file, the cutoff and delr (Verlet neighbour list shell) parameters. However, this dramatically increase the time required for simulation. Also, a second possibility is to compress the gas at a slightly elevated temperature (400-450 K) to avoid liquid clusters condensing separately. In doing this droplets formed from the rapid compression from a gas to a liquid will merge.

Figure 17: A snapshot of the model diesel condensed to liquid state density. Note that molecules wrap round the periodic boundary conditions (density calculated:  $0.83 \text{ g cm}^{-3}$ ).



Finally, a simulation for 1,000,000 steps were carried out in the  $NpT$  ensemble using the Nse-Hoover thermostat and barostat and a pressure of 1 atm, room temperature (298 K) using a leap frog algorithm. The aim was to arrive at equilibrium at a point where the density of our model diesel system could be similar to that of real liquid diesel.

Table 13: Parameters of the four simulations of the model liquid diesel from a gas phase to a liquid phase carried out in order to achieve equilibrium in the system.

	T / K	P / Katm	Step	Time step / fs	cutoff / Å	delt / Å
First	298.0	1.000	1,000,000	2	7.000	20.00
Second	398.00	10.00	1,000,000	2	10.00	45.00
Third	450.00	10.00	1,000,000	2	10.00	45.00
Fourth	298.00	0.001	1,000,000	2	8.000	3.000

## 7.1 Results from the model liquid diesel simulation

In order to verify that equilibrium is achieved we plot the ensemble average of the following thermodynamic properties: volume, total energy. It can be seen from figures 18 and figure 19 that the curves all increase during equilibration, but that the volume, total energy averages reach a steady state. The final mean density of our model liquid diesel is  $0.83 \text{ g cm}^{-3}$ , which is in very good agreement with the experimental density for a typical diesel of  $0.85 \text{ g cm}^{-3}$ .

Figure 18: Volume as a function of time for an equilibration run of the model diesel system at 1 atmosphere and 298 K, illustrating compression from an initial low density lattice configuration.

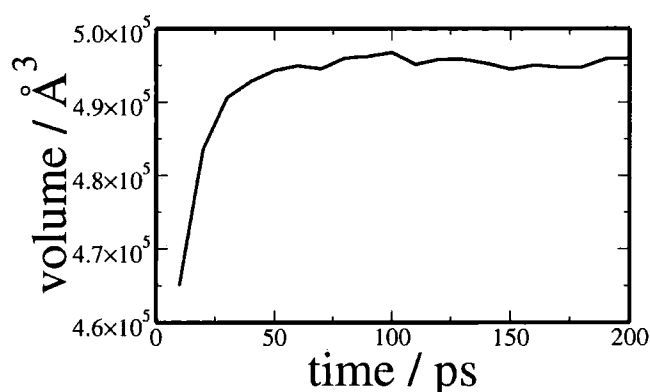
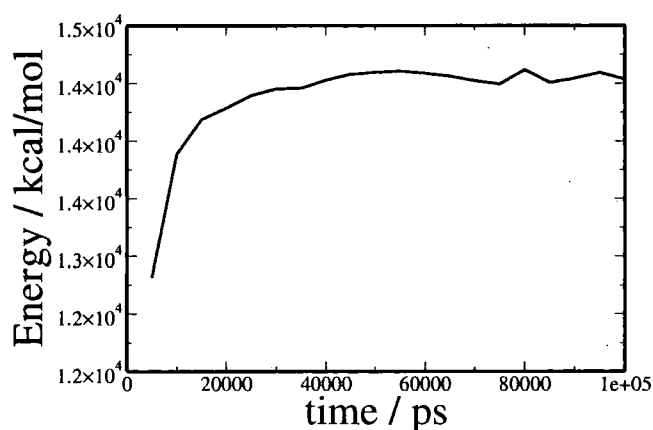


Figure 19: Total energy as a function of time for an equilibrium run of the model diesel at 1 atmosphere and 298K, during compression from an initial low density lattice configuration.



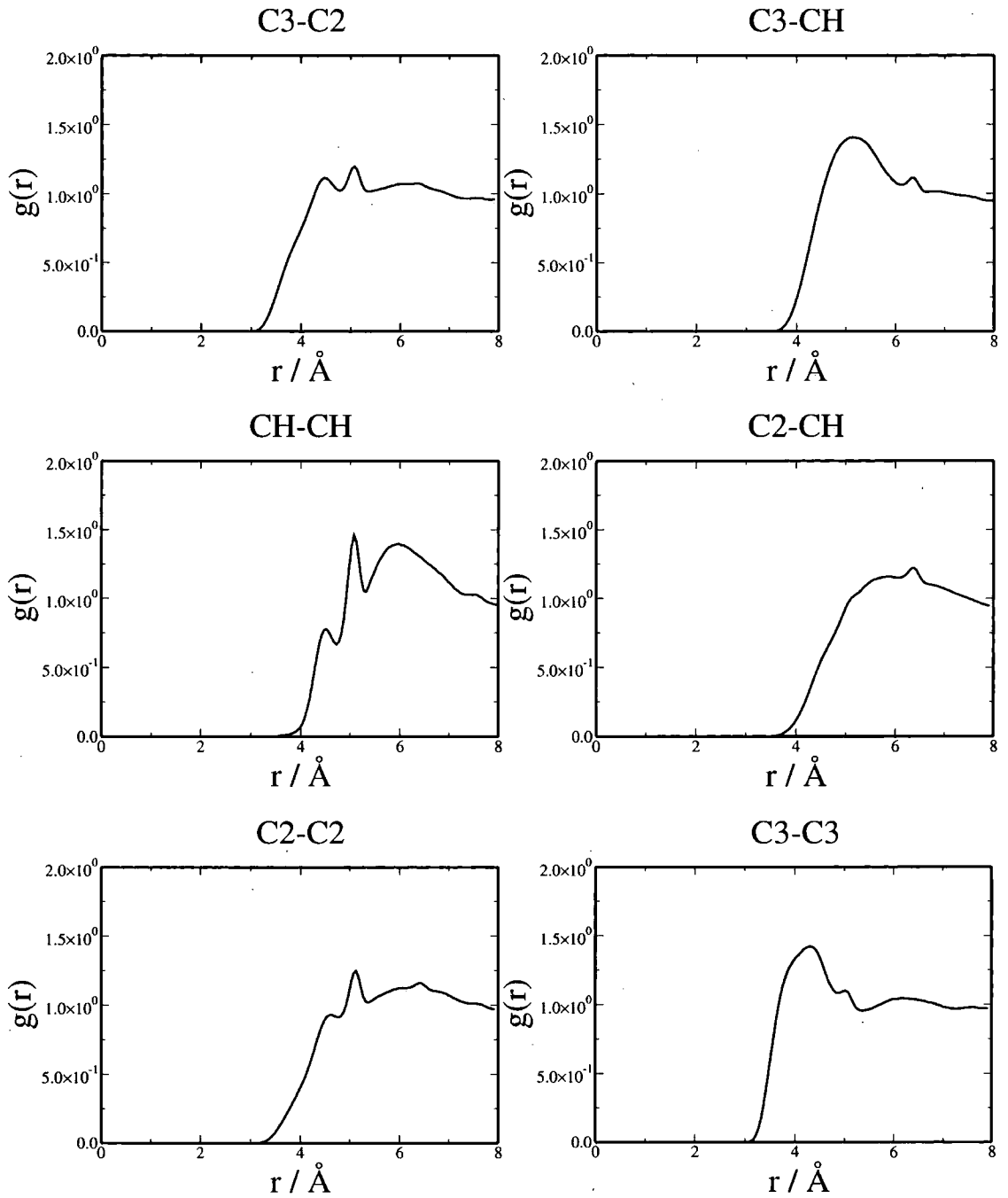
Radial distribution functions (RDFs) are pair correlation functions, which describe how the atoms in a system are packed around each other. This provides a particularly effective way of describing the average structure of a disordered molecular system such as a liquid. We have to think that the molecules are in constant motion, so the notion of a liquid structure has only got meaning in an average sense. In other words, the RDF is a measure of the probability of finding particles at a distance  $r_{ij}$  from each other. For a simple liquid the RDF is termed  $g(r_{ij})$ , where  $r_{ij}$  is the separation between atoms  $i$  and  $j$ .  $g(r_{ij})$  is defined as

$$g(r_{ij}) = \frac{V}{N^2} \langle \delta(r - r_{ij}) \rangle, \quad (50)$$

where  $\delta(r)$  is the Dirac delta function. The  $\frac{V}{N^2}$  prefactor normalizes the RDF relative to an ideal gas of the same density. A typical RDF plot shows a number of features: a) at short separation the RDF is zero, b) peaks indicate that the atoms pack around each other in a shell of neighbours. The occurrence of peaks at long range indicates a high degree of ordering.

The fact that the RDFs do not change significantly during the final part of the simulation is another indication that equilibration has been achieved.

Figure 20: Radial distribution function of each of the different interaction types in our liquid diesel model.



Four main conclusions can be drawn, as it has been shown in figure 20, from the RDF curves.

The CH groups cannot approach as closely as C2 groups or C3 groups because they always occur at branching points along the chain.

The  $\text{CH}_3$  groups occur as the terminal group of a chain and therefore approach more closely than  $\text{CH}$  and  $\text{CH}_2$  approach, as illustrated in the  $\text{CH}_3$ -  $\text{CH}_3$  RDF.

The  $\text{CH} - \text{CH}$  picks up the intramolecular interaction from along the chain, this is the reason why a sharp pick is found.

An other important property that allows us to verify that equilibrium has been achieved is the dihedral angle distribution of the branched solvent in our model liquid diesel for different torsional angles. The dihedral angle distributions and the relative percentages of trans-gauche conformations of the solvent are shown in figure 22 and in table 14. The chemical structure of the solvent is shown in figure 21.

Figure 21: Chemical structure of the solvent, the 2,4,6,10 tetramethyl dodecane showing the dihedral angles

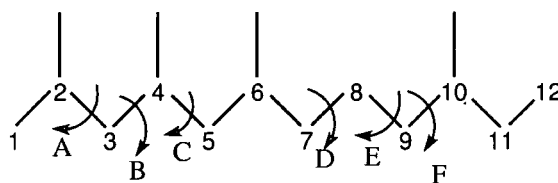


Figure 22: Dihedral angle distribution of different angles of the solvent in our model liquid diesel

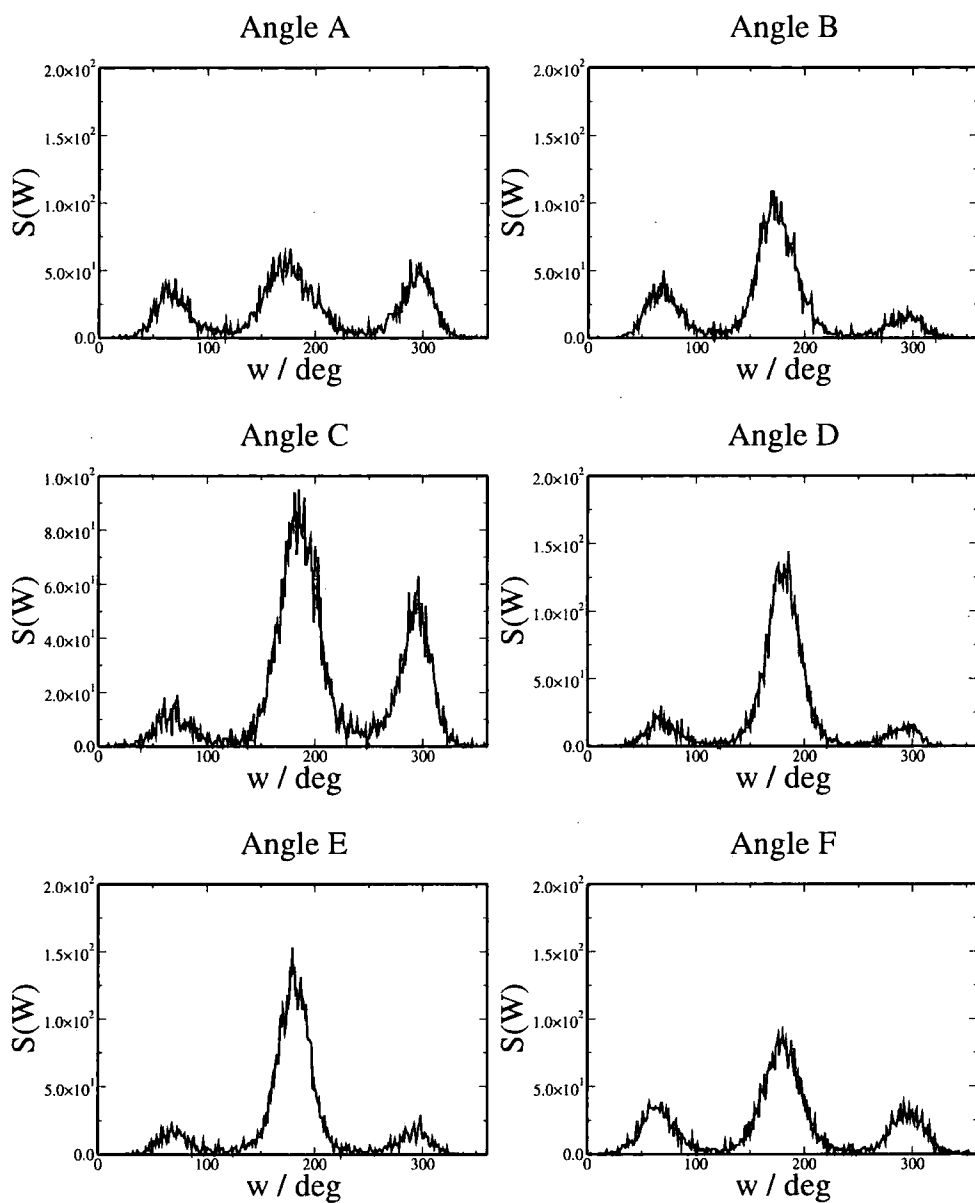


Table 14: Trans-gauche relative percentages for dihedral angles within the solvent in our model liquid diesel. Definition of angles are given in figure 21.

	Angle A	Angle B	Angle C	Angle D	Angle E	Angle F
Gauche - (%)	22.15692	22.64930	8.21156	11.54702	10.38754	22.45870
Trans (%)	48.22109	66.62960	61.37220	80.01905	78.875476	57.38564
Guache - (%)	29.62198	10.72109	30.41613	8.43392	10.736975	20.155654

As the solvent is a branched alkane (2,4,6,10 tetramethyl dodecane) in position 2, 4, 6 and 10 of the dodecane, from the figure 22, the result of the dihedral distribution angle are in good agreement with our expectations. If we look, for example, at the angle D formed by the atoms 6, 7, 8 and 9, the gauche+ and the gauche- have more or less the same relative percentages as we expect for this dihedral, which contains no branched groups. The same is true for the angle E, formed by the atoms 7, 8, 9 and 10 where the branched group is in position 10. On the other hand, for the dihedrals A, B and F the relative percentages of the gauche- and gauche+ are quite different due to the presence of the branched methyl group in the middle of the dihedral angle.

All the properties described above allow us to say that the simulation of our liquid model diesel led to an equilibrated system. This model can now be used for further simulations with the polymer EVA and the crystal C<sub>23</sub>.

## 8 Wax Crystal Modifier (EVA)

Wax Crystal Modifier (WCMs) all contain polyethylene-like segments and most can be classified within three main groups.

### 8.0.1 Random co-polymers

These are ethylene vinyl ester co-polymers, the most notable example is ethylene vinyl acetate (*EVA*). *EVA* is one of the most effective wax crystal growth inhibitors modifying the PP and the cold filter plugging point CFPP (PP and CFPP depressants) but not CP.

These co-polymers are believed to adsorb selectively onto the growing face of the crystal via the polyethylene backbone with the acetate and short alkyl groups extending into the fuel [41]. This adsorption and mode of action of this additives is not very selective but is efficient because of the polymer multipoint contact.

### 8.0.2 Comb type polymer.

There are several variations of this type of WCM. They are characterized by long *n*-alkyl side groups that protrude from the backbone, which can co-crystallize with the *n*-alkanes. Examples of this type of polymer include esters of fumaric acid co-polymerized with vinyl acetate (*FVA*) and poly-*n*-alkyl-methacrylates.

Different chain lengths can be used for the comb branches and those with between twelve and eighteen carbon atoms are generally favoured. These additives effect the cloud point (CP depressants) and also provide antisetling effects for the crystallised *n*-alkanes.

### 8.0.3 Nucleators

These additives are low molecular weight polymers. Typical examples are polyethylene glycol (PEG) esters, which have been esterified with docosanoic acid. These additives do not modify the crystal habit of the wax but increase the number of wax crystals present in the fuel compared to untreated fuel.

Unfortunately, some incompatibilities occasionally exist with regards to EVA type additives (which are CFPP and PP depressants) and *FVA* type additives (which are CP depressants). Ideally the aim is to find multifunctional additives that improve the CFPP, PP, CP and also give antisetling properties [42], [1].

## 8.1 Characteristics of EVA

EVA is a random co-polymer of ethylene vinyl acetate and there is little precise information with regard to detailed molecular structure, particularly regarding the distribution of co-monomer units. A linear EVA structure is found to be more effective as a wax crystal modifier. In order to achieve this [43], monomers have been used which possessed an acetate group such as 1-acetoxy-4,8-cyclododecadiene. Ring opening polymerization followed by hydrogenation for these, yield an EVA type polymer.

Free radical polymerised ethylene and EVA suffer backbiting. So random butyl side groups are obtained in addition to random vinyl acetate branches that break

up the polymethylene run where  $M_n$  (by VPO, i.e absolute) c.a. 2,500 and  $M_n/M_w$  2.2; we target EVA as made of 15 mole % of vinyl acetate and side chain branches of 4 per 100 backbone methylenes (measured by H-NMR) which is approximately 64 to 67 mole % of ethylene and 6 to 8 mole % hexene.

## 8.2 Force Field Parameters of EVA

Until now we have only used hydrocarbons in our simulations, but EVA is a copolymer (terpolymer) of ethylene vinyl acetate. The vinyl acetate group is an ester; the esters are functional derivatives of carboxylic acids where the hydroxyl (-OH) group is replaced by an alkoxy (-OR). TraPPE-UA force field parameters for the esters group in EVA molecule have been developed [44]; Lennard-Jones parameters for the methyl pseudo-atom were taken from the TraPPE-UA alkane parameters set [33], the carbonyl carbon parameters were taken from carboxylic acid [45], the carbonyl oxygen from carbon dioxide model [46] and the ether oxygen from the ether parameter set [47]. These are illustrated in table 15-19.

Table 15: 1-2 Interaction [Stretch]

Stretch Type	Distance / Å
CH <sub>x</sub> -CH <sub>y</sub>	1.540
C=O	1.200
C-O	1.344
C-CH <sub>3</sub>	1.520
CH-O	1.410

Table 16: 1-3 Interaction [Bend]

Bend Type	$\theta$ / degree	$(K_\theta/k_B)$ / K
CH <sub>x</sub> -(CH)-CH <sub>y</sub>	112.0	62,500.00
O-C-CH <sub>3</sub>	110.0	70,600.00
O=C-CH <sub>3</sub>	125.0	62,500.00
O-C=O	125.0	62,500.00
CH <sub>x</sub> -CH <sub>y</sub> -O	112.0	50,300.00
CH-O-C(=O)	110.0	70,600.00

Table 17: 1-4 Interaction [Torsion]

Torsion Type	$c_1 / k_B / K$	$c_2 / k_B / K$	$c_3 / k_B / K$
CH <sub>x</sub> -(CH <sub>2</sub> )-(CH <sub>2</sub> )-CH <sub>y</sub>	355.03	-68.19	791.32
CH <sub>x</sub> -(CH <sub>2</sub> )-(CH)-CH <sub>y</sub>	428.73	-111.85	441.27
CH <sub>x</sub> -CH <sub>y</sub> -O-C	725.35	163.75	558.20
CH <sub>x</sub> -O-C=O	2194.00	2059.0	-153.4
CH-O-C-CH <sub>x</sub>	993.1	520.7	-138.5
CH <sub>x</sub> -CH <sub>2</sub> -CH <sub>2</sub> -O	172.62	-53.34	769.93

Table 18: Lennard Jones 12-6 parameters

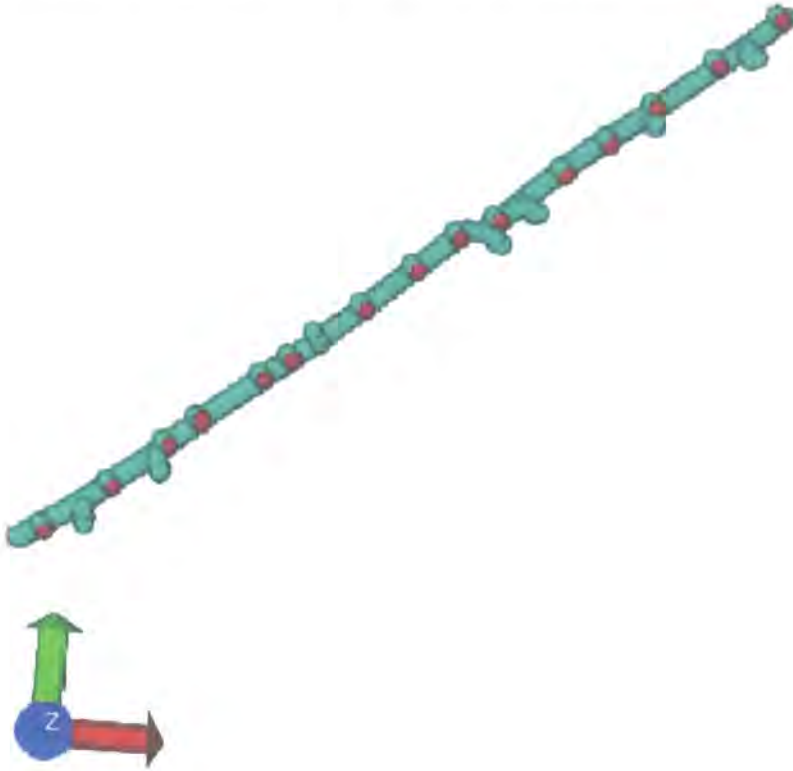
Atom Type	$(\epsilon / k_B) / K$
[CH <sub>3</sub> ]-CH <sub>x</sub>	98.00
[CH]-(CH <sub>3</sub> ) <sub>3</sub>	10.00
CH <sub>x</sub> -[CH <sub>2</sub> ]-CH <sub>y</sub>	46.00
-O-	55.00
C=O	41.0
=O	79.00

Table 19: Partial charges used in EVA simulation

Atom Type	$q / e$
-O-	-0.4
C=O	0.55
=O	-0.45
CH <sub>3</sub> -(C)	0.05
CH-O	0.25

The polymer EVA was draw with a molecular modeling program, Maestro.

Figure 23: An extended EVA chain drawn with Maestro molecular modelling software, before starting the simulation. Notice the random distribution of the vinyl acetate group and the butyl group in the long chain polymer.



As a polymer is a large molecule, there are a huge number of conformations. It proved convenient to start from an extended conformation and then use MD to allow the polymer chain to curl up and provide a better starting configuration to put into the diesel solution.

After creating the FIELD, the CONFIG file and the CONTROL file, a first MD simulation in a canonical ensemble was carried out without periodic boundary condition with the following characteristics:

Table 20: Summary of the first EVA MD simulations

$T / \text{K}$	$p / \text{atm}$	Step	Time step / fs	cutoff / Å	delr / Å
298.00	1.00	50,000	2	100.00	30.00

A snapshot of EVA at different time steps of the simulation were taken as shown in figures 24-26. At the end of the simulation the polymer remained stable in a coil arrangement, as expected from entropic considerations.

Figure 24: EVA snapshots from a gas phase MD simulation

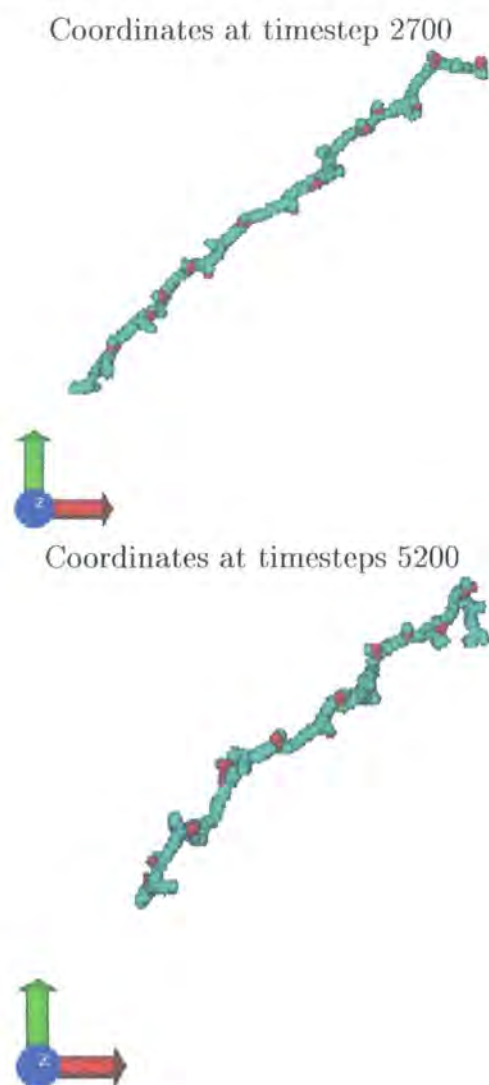
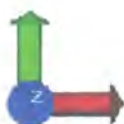
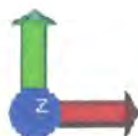
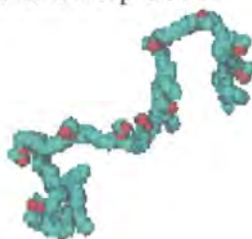


Figure 25: EVA snaphops from a gas phase MD simulation

Coordinates at timestep 20100



Coordinates at timestep 30300

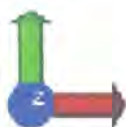


Coordinates at timestep 42700

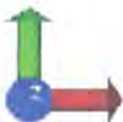


Figure 26: EVA snapshots from a gas phase MD simulations

Coordinates at timestep 48200



Coordinates at timestep 49000



### 8.3 A property of EVA polymer: radius of gyration

The three dimensional structure of a polymer chain such as EVA can determine many of its most important properties. One of these properties is the radius of gyration.

The mean radius of gyration  $R_g$  [48]- [49] of a polymer chain is defined as the root mean squared distance of the chain segment from the centre of mass of the chain.

It is calculated using

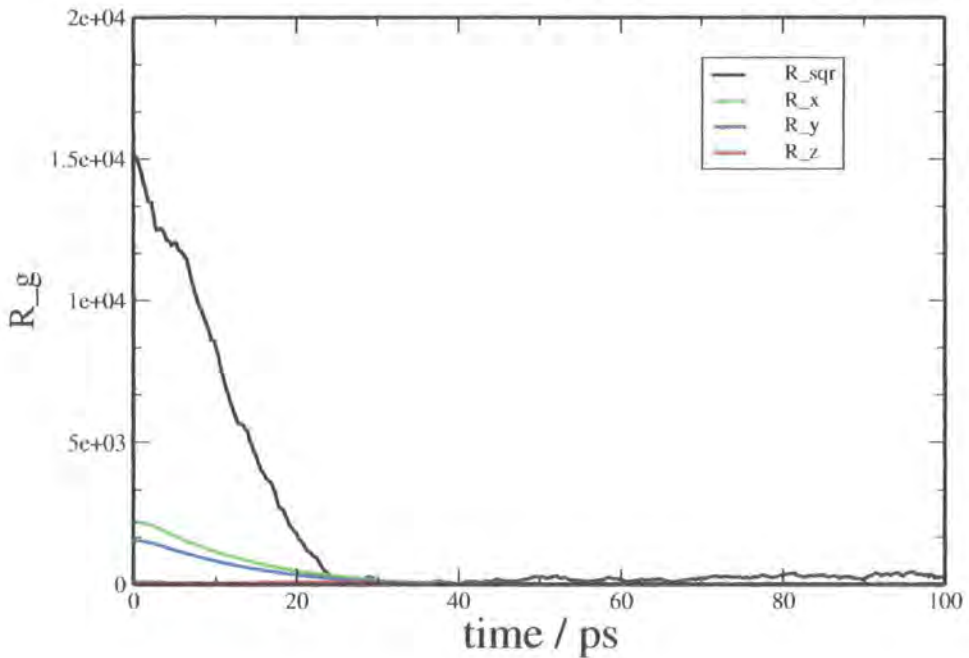
$$R_g = \sqrt{\frac{\sum_i^N (\mathbf{r}_i - \mathbf{r}_{cm})^2}{N}} \quad (51)$$

where  $\mathbf{r}_i$  is the  $i^{th}$  monomer position and  $\mathbf{r}_{cm}$  is the positions of the centre of mass.

The radius of gyration represents the overall size and shape of the polymer chain. For a given  $N$ , low values of  $R_g$  represent more compact folded configurations; and higher values of  $R_g$  represent unfolded configuration. In other words, the natural process of curling up of EVA can be measured quantitatively by calculating the radius of gyration, the radius of gyration squared and its components in the  $x, y, z$  direction.

From the first MD simulation the radius of gyration squared and its components in  $x, y, z$  direction were plotted as a function of simulation time.

Figure 27: Radius of gyration squared and  $x, y, z$  components plotted against the simulation time.



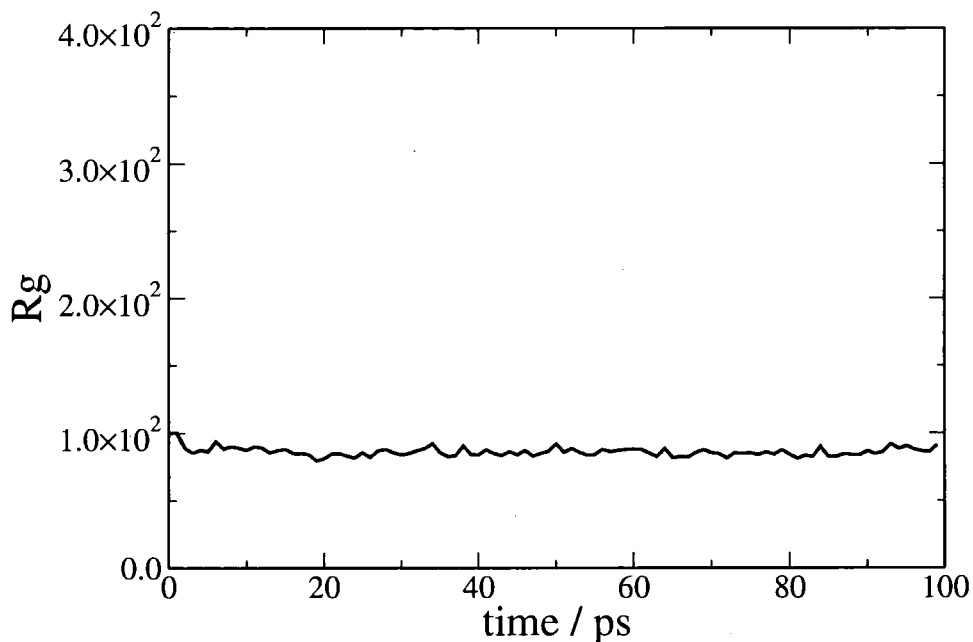
From figure 27 the curves show a reduction in the radius of gyration as a function of simulation time as one would expect from the snapshots of figure 24-26.

Starting from the last configuration of the previous run, a longer MD simulation was carried out in the canonical ensemble, with the characteristics given in table 21.

Table 21: Parameters of the second EVA gas phase MD simulation.

$T / \text{K}$	$p / \text{atm}$	Step	Time step / fs	cutoff / $\text{\AA}$	delr / $\text{\AA}$
298.00	1.00	500,000	2	100.00	30.00

Figure 28: Mean value of the radius of gyration of EVA as an “equilibrated” chain polymer in a gas phase.

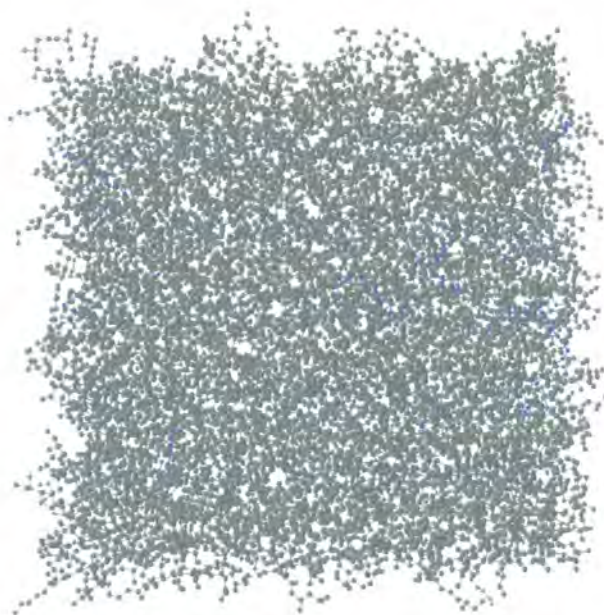


This simulation is made in order to check the equilibration with regards to the natural process of curling up of this polymer; a converged ensemble average for the radius of gyration of EVA in the gas phase is shown in the figure 28. The average values of  $R_g$  of EVA in the gas phase is 86.14  $\text{\AA}$ .

It is also possible to consider the radius of gyration of a polymer chain like EVA in a solvent. Whether the solvent is a good or bad one for EVA will determine whether the radius of gyration will become larger or smaller when immersed in the solvent.

In our case the solvent is the model diesel previously studied. In order to merge the model diesel with EVA, we need to unperiodically box our diesel as shown in figure 29. This will allow the EVA to see full molecules, not only a part of those that they are split via the periodic boundaries.

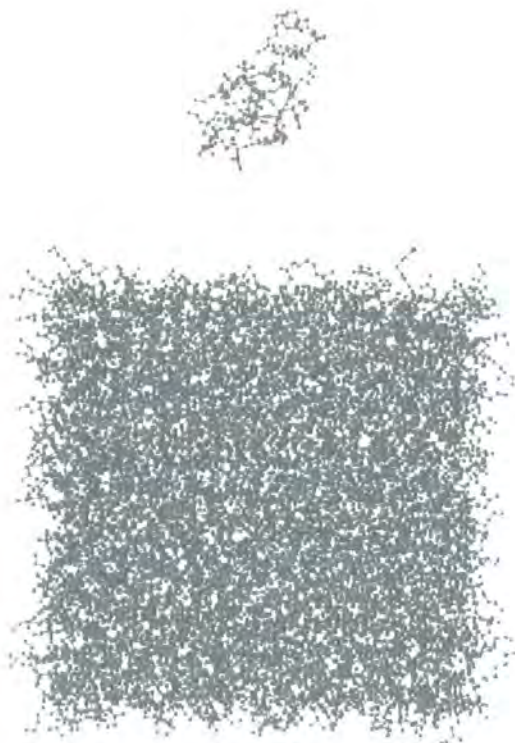
Figure 29: Snapshot of the model diesel condensed to liquid state density. This snapshot shows unperiodically boxed diesel molecules, so that individual molecules are not split by being wrapped round the periodic boundary conditions. .



## 9 EVA + Diesel

Starting from the final configuration of the equilibrated EVA, the liquid model diesel and the polymer EVA were merged and the starting configuration of the system (diesel + EVA) is shown in figure 30.

Figure 30: Starting configuration of the system made using our model diesel plus the EVA polymer



In order to compress the system quickly from gas to the liquid phase, two initial  $NpT$  molecular dynamics simulations, using the Nose-Hoover thermostat and barostat, were carried out with the characteristics described in table 22.

Table 22: Conditions for a molecular dynamics simulation for EVA plus our model liquid diesel.

$T / \text{K}$	$p / \text{atm}$	Step	Time step / fs	cutoff / Å	delr / Å
298	1000	1,000	2	25.00	30.00
298	1000	10,000	2	25.00	30.00

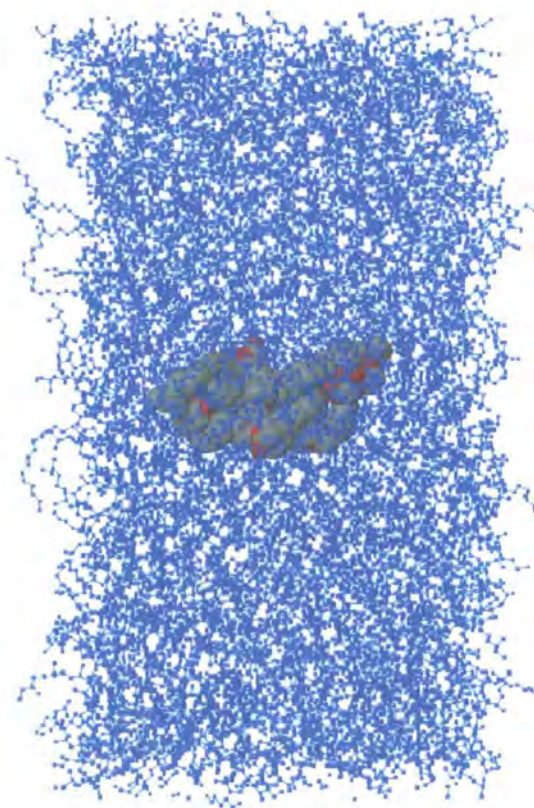
After compressing at high pressure, relaxation of the system was performed with a long molecular dynamic simulation at 1 atm with the details shown in table 23.

Table 23: Molecular dynamic simulation of the system EVA + our liquid model diesel after compressing the system.

$T / \text{K}$	$p / \text{atm}$	Step	Time step / fs	cutoff / Å	delr / Å
298	1	1,000,000	2	8	3

The final configuration of the equilibrated system of EVA plus diesel is shown in figure 31.

Figure 31: Equilibrated system of EVA plus our liquid model diesel: shapshot of the final configuration where the system was unbox and EVA was shifted at the center of the box .



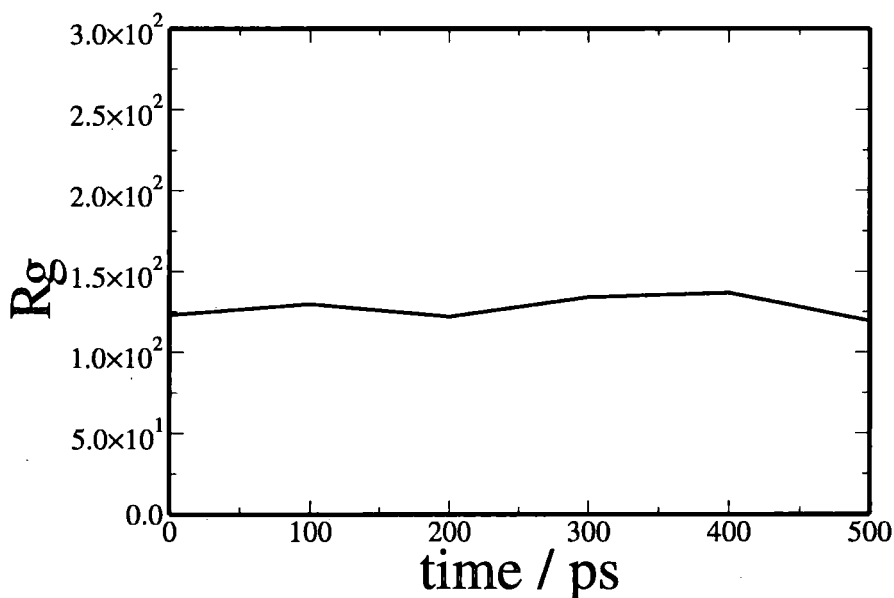
From figure 31, it can be seen that complete solvation of the EVA by the diesel has been achieved.

## 9.1 Results for EVA plus diesel

In order to understand if the diesel is a good or bad solvent for the polymer EVA, the radius of gyration of the EVA in diesel was calculated. In general, for a polymer chain it is crucial to verify in which solvent the polymer is dissolved. For good solvents the chain is more expanded while for bad solvents the chain segments stay close to each other. This means that if diesel is a good solvent for EVA, the radius of gyration will become larger [50].

The radius of gyration of EVA in the liquid diesel solvent is shown in figure 32.

Figure 32: Radius of gyration of the EVA polymer in the liquid diesel solvent plotted as a function of simulation time in ps.



From this graph the radius of gyration of the EVA polymer when it is in the liquid diesel solvent is plotted versus the simulation time.

The average radius of gyration of EVA in the gas phase is 86.14 Å, while the average value of EVA in the liquid diesel is 127.55 Å.

As the radius of gyration of EVA increases while it solvated in the diesel solvent, we can define our liquid model diesel as a good solvent for the polymer EVA.

## 10 Crystal

### 10.1 n-alkanes crystals

*n*-alkanes crystallize to form thin plates with regular faces in which the chain direction is more or less perpendicular to the lamella surface. A combination of single crystal and powder X-ray diffraction analysis has enabled some of these system to be characterized. In the low temperature modifications, three solid-state structures have been identified:

TRICLINIC:  $6 \leq n(\text{even}) \leq 26$

MONOCLINIC:  $28 \leq n(\text{even}) \leq 36$

ORTHORHOMBIC  $\geq 36$  and  $n(\text{odd})$

In all the structures the hydrocarbon chains are linear and they have trans configurations. The chains are parallel to one another, the terminal methyl groups forming the surfaces of lamella.

### 10.2 C<sub>23</sub> crystal

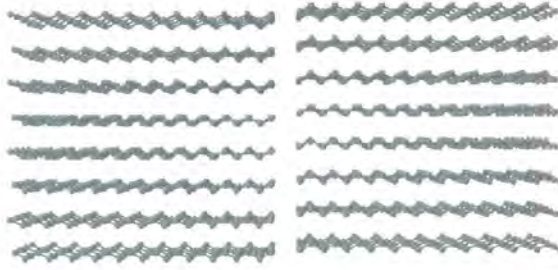
Infinuem Ltd. have collaborated with different Universities to investigate the structure of individual and mixed *n*-alkane crystals. Dr S. Craig from the University of Strathclyde [51], presents crystallographic unit cell parameters and fractional coordinates for a series of *n*-alkane crystal systems (C<sub>13</sub>H<sub>28</sub> to C<sub>60</sub>H<sub>28</sub>) and from it, unit cell parameters of C<sub>23</sub>H<sub>48</sub>, as shown in table 24, allow us to build a crystal structure with a molecular modeling program (Cerius2). The C<sub>23</sub>H<sub>48</sub>, called tricosane has a typical orthorhombic structure with  $P_{bcm}$  space group.

Table 24: Unit cell parameters of C<sub>23</sub>.

$a / \text{\AA}$	$b / \text{\AA}$	$c / \text{\AA}$	$\alpha / \text{deg}$	$\beta / \text{deg}$	$\gamma / \text{deg}$
4.967	7.441	62.189	90.000	90.000	90.000

A single crystal of C<sub>23</sub> was build. The cell was duplicated in the *a* and *b* direction in order to have 64 molecules of C<sub>23</sub>.

Figure 33: Crystal  $C_{23}$  before the simulation .



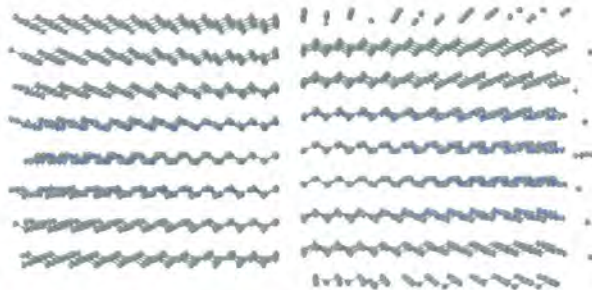
A MD simulation was carried out at 100 K in the  $NVT$  ensemble with the following characteristics:

Table 25: Parameters of a molecular dynamic simulation of 64 molecules of  $C_{23}$  orthorhombic crystal.

$T / K$	$p / atm$	Step	Time step / fs	cutoff / Å	delr / Å
100.00	1.00	1,000,000	2	8.50	1.00

At the end of the simulation the crystal remained stable and this was a good starting point for merging the crystal with the model diesel and the EVA.

Figure 34: Figure of the crystal  $C_{23}$  after the simulation (Note atoms at the end of the cell are broken across the periodic boundary conditions).



## 11 Model Diesel plus Crystal simulations

After creating the right FIELD, CONTROL and CONFIG files (unperiodic CONFIG), a 100 steps simulation of the liquid model diesel plus the C<sub>23</sub> crystal was carried out in order to compress the system from a gas phase to a liquid one, followed by 20000, 100000 and 1 million step runs in an *NVT* ensemble with the characteristics described in table 26.

Table 26: Parameters of the first series of simulations in *NVT* ensemble of our liquid model diesel plus the C<sub>23</sub> crystal.

$T / \text{K}$	$p / \text{atm}$	Step	Time step / fs	cutoff / Å	delr / Å
298.00	1.00	100	2	25.00	10.00
298.00	1.00	20,000	2	25.00	10.00
298.00	1.00	100,000	2	25.00	10.00
298.00	1.00	1,000,000	2	25.00	10.00

Figure 35: Snapshot after the first simulation (100 steps) of the model liquid diesel and the  $C_{23}$  crystal. (Note atoms at the edge of the cell are broken across the periodic boundary conditions).

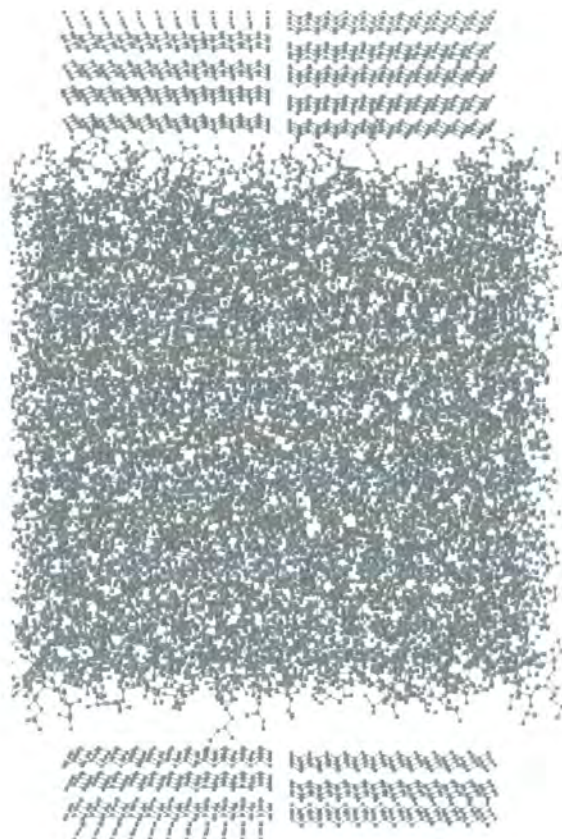
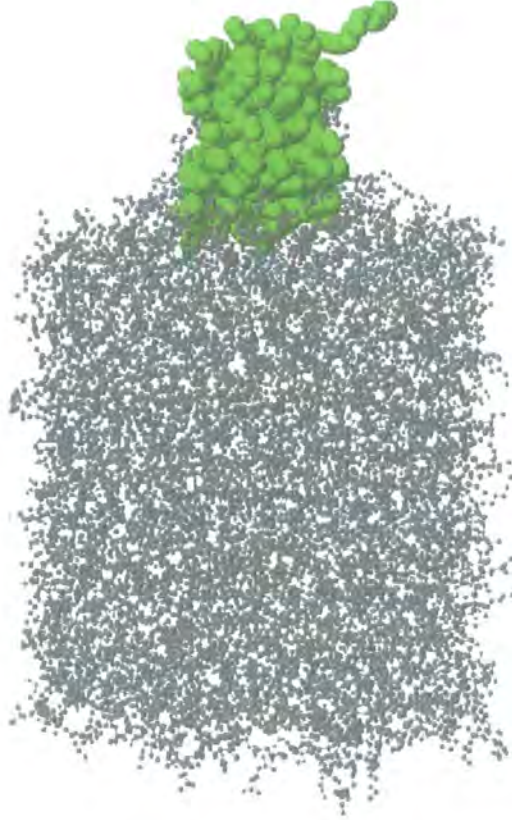


Figure 36: Snapshot after the last simulation in the  $NVT$  ensemble of the model liquid diesel and the  $C_{23}$  crystal (notice that they are still gaps in the system).  $t+\delta t$



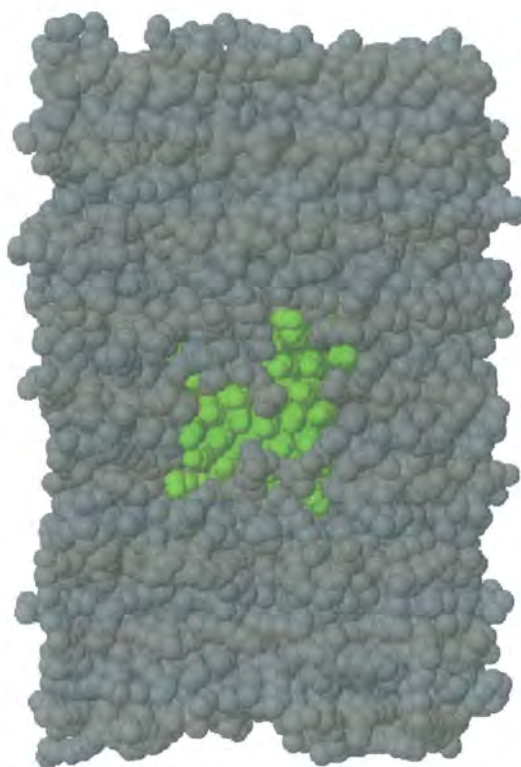
In order to fill the space between the two merged systems, a series of simulations in  $NpT$  ensemble at high pressure were carried out using the conditions shown in table 27.

Table 27: Parameters of a series of simulation in  $NpT$  ensemble at high pressure of the model liquid diesel plus the  $C_{23}$  crystal.

$T / K$	$p / atm$	Step	Time step / fs	cutoff / Å	delr / Å
298	1000	10,000,000	2	25.00	10.00
298	1000	10,000,000	2	8.50	3.00

When a rapid compression at high pressure was made, the crystal is completely incorporated inside of the liquid diesel, as shown in the shapshot at figure 37.

Figure 37: Snapshot of the model liquid diesel plus the  $C_{23}$  crystal after rapid compression at high pressure in the  $NpT$  ensemble.



## 12 Model Diesel plus Crystal plus EVA

After creating the right FIELD (FIELD of diesel plus FIELD of crystal plus FIELD of EVA), CONTROL and CONFIG files, a 100 steps simulation of the liquid model diesel plus the  $C_{23}$  crystal were carried out, followed by 20000, 100000 and 1 million step runs in the  $NVT$  ensemble with the characteristics show in table 28.

The starting configuration shapshot is shown in figure 38.

Figure 38: Snapshot of the final simulation carried out for the model liquid of diesel plus crystal plus EVA.

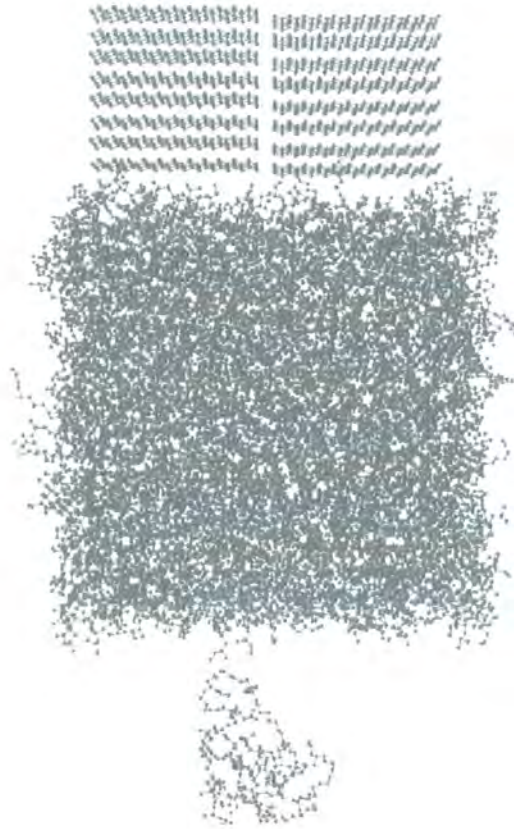


Table 28: Parameters of  $NVT$  ensemble simulations, carried out for the mixture model diesel plus crystal plus EVA.

	$T / \text{K}$	$p / \text{atm}$	Step	Time step / fs	cutoff / $\text{\AA}$	delr / $\text{\AA}$
First	298.0	1,000	100	2	35.00	30.00
Second	98.00	1,000	20,000	2	35.00	30.00
Third	298.00	1,000	20,000	2	20.00	25.00
Fourth	298.00	1,000	1,000,000	2	8.00	3.00

In these initial simulations, the  $NVT$  ensemble allows system to relax any initial stress without the added complexity of a barostat. Therefore avoiding any rapid fluctuations in box size, which might occur at constant pressure. The results in figure

39 show that the diesel starts to melt the surface of the crystal but there remains a large gap in the system. The latter can then be removed with a quick compression at high pressure in the  $NpT$  ensemble simulations, followed by equilibration of the system with 1 atm  $Npt$  simulations; as summarized in table 29.

Figure 39: Snapshot of the final configuration of the  $NVT$  simulations described in table 28.

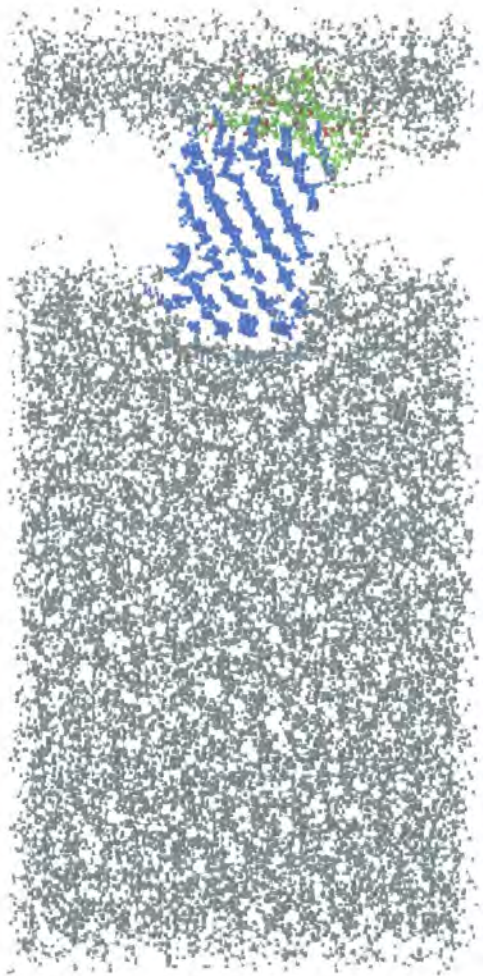
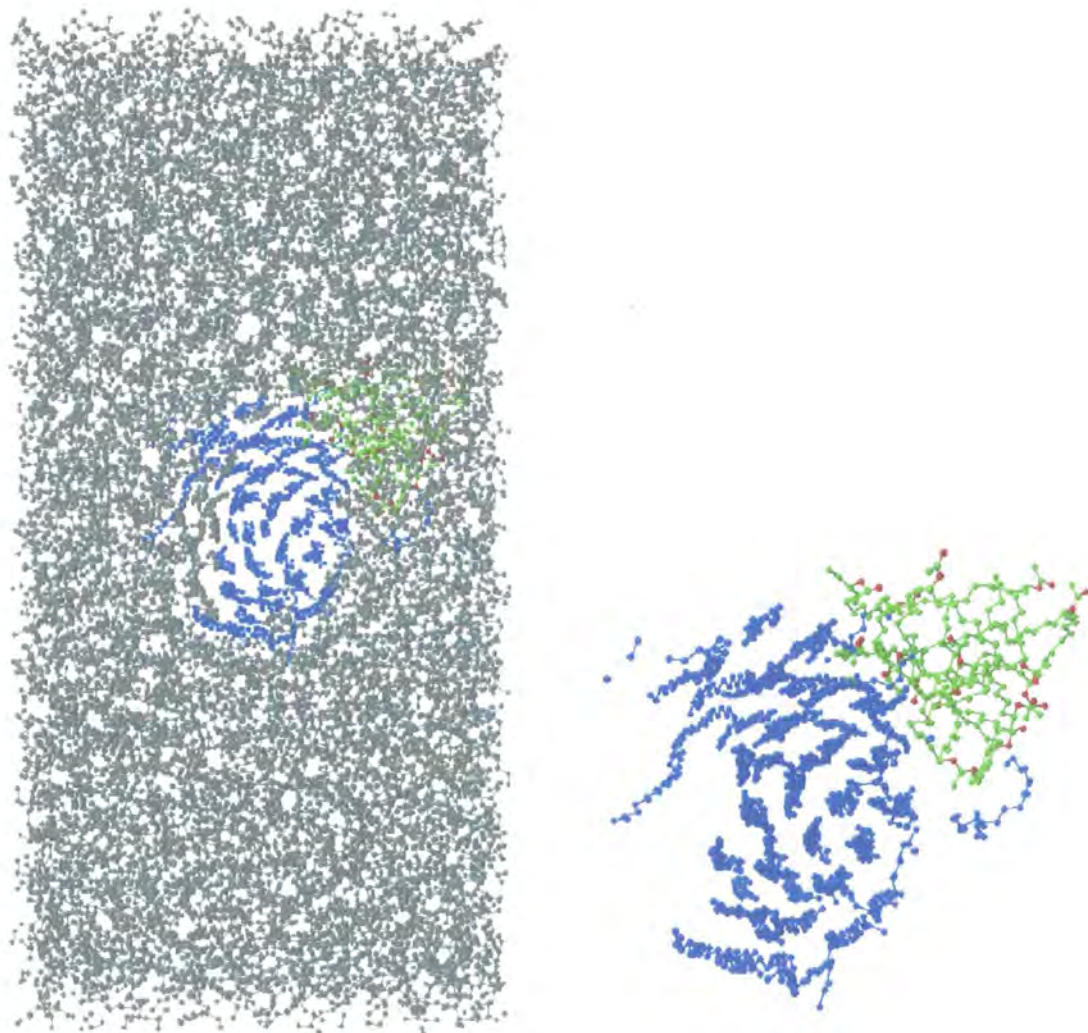


Table 29: Parameters for  $NpT$  simulations of diesel plus crystal plus EVA.

	$T / \text{K}$	$p / \text{atm}$	Step	Time step / fs	cutoff / Å	delr / Å
First	298	1,000	1,000,000	2	20.00	25.00
Second	298	1,000	1,000,000	2	8.00	3.00
Third	298	1	1,000,000	2	8.00	3.00

A Snapshot of the final  $NpT$  simulation where the gaps have been filled is shown in figure 40. Here the diesel is shown in grey, the crystal in blue and the EVA is green with the red atom of oxygen on EVA.

Figure 40: Snapshot of the final  $NpT$  simulation at 1 atm in order to relax the system (note that now all the gaps between the different components of the system have been filled).



The snapshot in Figure 40 shows that at this temperature the edge of the crystal has started to melt into the surrounding diesel liquid but that the centre of the crystal has remained crystalline. The EVA was found to migrate to the surface of the crystal, as shown in the snapshot on the right of Figure 40, which shows the molecules of diesel removed.

## 13 Conclusion

A simulation of hexane was carried out with different force fields in order to decide the most appropriate one to be used for a model of diesel. The TraPPE force field was selected due to good agreement with experimental data and due to availability of additional parameters (e.g. not only hydrocarbons) for other functional group in addition to hydrocarbons, as used later for EVA (e.g. esters groups).

A model diesel was created composed of 78.7 % of a solvent (2,4,6,10 tetramethyl dodecane) plus a distribution of *n*-alkanes from C<sub>10</sub> up to C<sub>26</sub>. In compressing from a gas phase to a liquid there was an initial formation of liquid droplets with space between them. The inhomogeneity of the system caused a major technical problem in the simulations, which was eventually solved by running simulations with a very large cutoff and Verlet list shell cutoff. This slowed down the simulations dramatically, but proved to be the only way to condense the clusters. Finally, after further equilibration this led to an equilibrium liquid diesel system in which the density was in good agreement with experiment. Volume, total energy and enthalpy / time graphs were plotted and the radial distribution function of all the atoms in the model diesel were monitored to check equilibrium. Also the dihedral angle distributions of the solvent molecules in the diesel system was studied for six dihedral angles. All those properties allowed us to say that the simulations of the liquid model diesel built, had produces an equilibrated system.

MD simulations of EVA, as a co-polymer of ethylene vinyl acetate with the TraPPE force field were carried out starting from an extended conformation. During the simulation the polymer chain curled up and remained stable in a coil configuration at the end of the simulation, as expected from entropic considerations. The radius of gyration, the radius of gyration squared and its components in the *x*, *y*, *z* directions, were plotted against time. The mean values of *R<sub>g</sub>* in the gas phase was found to be 86.14 Å.

After unperiodically boxing the liquid model diesel, it was merged with the EVA polymer, starting with the final configuration of the equilibrated system. This simulations was made to understand if the diesel can be considered as a good or bad solvent for EVA. The mean radius of gyration when it was immersed in the diesel

was found to be of 127.55 Å, showing an increase compared to EVA in gas phase. We can conclude that diesel can be considered a good solvent for EVA.

To model the *n*-alkanes crystals, an orthorhombic structure with  $P_{bcm}$  space group for  $C_{23}H_{48}$ (tricosane) was built with a Cerius2 molecular modeling program. MD simulations of the diesel plus  $C_{23}$  crystal were carried out leading to a crystal system completely incorporated inside of the diesel.

Different simulations of the three components systems of diesel plus crystal plus EVA were performed at 298 K. Here the edge of the crystal was found to melt into the surrounded liquid diesel leaving the centre of the crystal crystalline.

## References

- [1] P. Claudy, J. M. Letoffe, B. Bonardi, D. Vassailakis, and B. Damin, *Fuel* **72**, 821 (1993).
- [2] G. I. Brown, R. I. Tack, and E. C. J: In *SAE Technical Paper Series*, 881652 (1988).
- [3] G. I. Brown, E.W. Lehmann, and K. Lewtas: In *SAE, Technical Paper Series*, 890031 (1989).
- [4] K Lewtas, R. D. Tack, D. H. M. Beiny, and J. W. Mullin: *Advances in Industrial Crystallisation*, chapter 5, page 166 (1991).
- [5] J. L. Hutter, H. E. King, and M. Y. Lin, *Macromolecules* **33**, 2670 (2000).
- [6] C. A. Koh, R. E. Westacott, W. Zhang, K. Hirachand, J. L. Creek, and A. K. Soper, *Fluid Phase Equilib.* **194**, 143 (2002).
- [7] M. E. Daley and B. D. Sykes, *Protein Sci.* **12**, 1323 (2003).
- [8] S. Grandum, A. Yabe, K. Nakagomi, M. Tanaka, F. Takemura, Y. Kobayashi, and P. E. Frivik, *J. Cryst. Growth* **205**, 382 (1999).
- [9] D. M. Duffy, C. Moon, and P. M. Rodger, *Mol. Phy.* **102**, 203 (2004).
- [10] D. M. Duffy and P. M. Rodger, *Phys. Chem. Chem. Phys* **2**, 4804 (2000).
- [11] W. Smith, C. W. Yong, and P. M. Rodger, *Molec. Simulat.* **28**, 385 (2002).
- [12] H. M. M. Shearer and V. Vand, *Acta Crystallogr* **9**, 379 (1956).
- [13] P. M. Morse, *Phys. Rev.* **34**, 57 (1929).
- [14] Frank Jensen: *Introduction to Computational Chemistry* (Wiley Editor, 1999).
- [15] J. E. Lennard-Jones: volume 106 of *A*, page 463 (1924).
- [16] J. R. Hill, *J. Chem. Phys.* **16** (1948).

- [17] Z. X. Wang, W. Zhang, C. Wu, H. X. Lei, P. Cieplak, and Y. Duan, *J. Comput. Chem.* **27**, 994 (2006).
- [18] B. Brooks, R. E. Bruccoleri, B. Olafson, D. States, S. Swaminathan, and M. Karplus, *J. Comp. Chem.* **4**, 187 (1983).
- [19] W. Van Gunsteren and A. Mark, *Eur. J. Biochem.* **204**, 947 (1992).
- [20] W. L. Jorgensen, J. D. Madura, and C. J. Swenson, *J. Am. Chem. Soc.* **106**, 6638 (1984).
- [21] J. H. Lii and N. L. Allinger, *J. Comput. Chem* **19**, 1001 (1998).
- [22] N. L. Allinger, *J. Am. Chem. Soc.* **99**, 8127 (1977).
- [23] N. L. Allinger, K. H. Chen, J. H. Lii, and K. A. Durkin, *J. Comput. Chem.* **24**, 1447 (2003).
- [24] N. L. Allinger and K. A. Durkin, *J. Comput. Chem.* **21**, 1229 (2000).
- [25] L. Verlet, *Phys. Rev.* **159**, 98 (1967).
- [26] A. R. Leach: *Molecular Modelling, Principle and Applications* (England, 2001).
- [27] D. Chandler: *Introduction of Modern Statistical Mechanics* (Oxford University Press, New York, 1987).
- [28] H. C. Anderson, *J. Chem. Phys.* **74**, 2384 (1980).
- [29] W. G. Hoover, *Phys. Rev. A* **31**, 1695 (1985).
- [30] S. Nosé, *J. Chem. Phys.* page 511 (1981).
- [31] H. J. C. Berendsen, J. P. M. Postma, W. F. VanGunsteren, A. DiNola, and J. R. Haak, *J. Chem. Phys.* **81**, 3684 (1984).
- [32] S. Toxvaerd, *Phys. Rev. E* **47**, 343 (1993).
- [33] M. G. Martin and J. I. Siepmann, *J. Phys. Chem. B* **102**, 2569 (1998).
- [34] M. G. Martin and J. I. Siepmann, *J. Phys. Chem. B* **103**, 4508 (1999).

- [35] J. I. Siepmann, M. G. Martin, C. J. Mundy, and M. L. Klein, *Mol. Phys.* **90**, 687 (1997).
- [36] S. K. Nath, F. A. Escobedo, and J. J. De Pablo, *J. Chem. Phys.* **108**, 9905 (1998).
- [37] S. K. Nath and R. Khare, *J. Chem. Phys.* **115**, 10837 (2001).
- [38] S. K. Nath and J. J. De Pablo, *Mol. Phys.* **98**, 231 (2000).
- [39] D. A. C. Compton, S. Montero, and W. F. Murphy, *J. Phys. Chem.* **84**, 3587 (1980).
- [40] D. L. G. Cheung: Ph.D. thesis, Durham University (2002).
- [41] I. G. Davidson and G. G. Cameron, *Macromolecules* **28**, 5964 (1995).
- [42] A. Rossi: In *SAE Technical Paper Series*, 890034 (1989).
- [43] Carole-Anne Smith: Ph.D. thesis, University of Durham (1993).
- [44] G. Kamath, J. Robinson, and J. J. Potoff, *Fluid Phase Equilibria* **240**, 46 (2006).
- [45] G. Kamath, F. Cao, and J. J. Potoff, *J. Phys. Chem. B* **108**, 14130 (2004).
- [46] J. J. Potoff and J. I. Siepmann, *AIChE J.* **47**, 1676 (2001).
- [47] J. M. Stubbs, J. J. Potoff, and J. I. Siepmann, *J. Phys. Chem. B* **108**, 17596 (2004).
- [48] M. K. Kosmas, *J. Phys. A-Math. Gen.* **14**, 2779 (1981).
- [49] D. T. Seaton, S. J. Mitchell, and D. P. Landau, *Brazilian J. Phys.* **36**, 623 (2006).
- [50] K. Terao and J. W. Mays, *European Polymer Journal* **40**, 1623 (2004).
- [51] S. R. Craig: Ph.D. thesis, University of Strathclyde (1995).

## Appendix A): Courses attended

- INTRODUCTION OF FORTRAN 90 by Prof. J. M. Hutson, Chemistry Department, Durham University. Test taken on 12th December 2005, Mark: 70/100
- NUMERICAL METHODS by Dr M. Wilson, Chemistry Department, Durham University. Test taken twice and passed with mark: 77/100.
- MANAGING YOUR RESEARCH PROJECT I. INTRODUCTION - 4 NOV 2005.
- THE KEY SKILLS AWARD FOR POSTGRADUATE RESEARCH STUDENTS I. INTRODUCTION - 11 NOV 2005.
- MANAGING YOUR RESEARCH PROJECT II. EFFECTIVE COMMUNICATION - 14 NOV 2005.
- MANAGING YOUR RESEARCH PROJECT III. PROJECT MANAGEMENT ESSENTIALS - 1 DEC 2005.
- MANAGING YOUR RESEARCH PROJECT IV. TIME MANAGEMENT - 10 FEB 2006.
- GIVING YOUR FIRST PRESENTATION: ORAL PRESENTATION SKILLS - 18 MAY 2006.

## Appendix B): Seminars attended

- Wednesday 2nd November: PROFESSOR JON A. PREECE, Nanoscale Chemistry Laboratory, School of Chemistry, University of Birmingham. "Chemical Nanoengineering".
- Wednesday 16th November: PROFESSOR IAN WILLIAMS, Department of Chemistry, University of Bath. "How do calculated kinetic isotope effects relate to transition state structure?".
- Wednesday 7th December : PROFESSOR JOHN SUTHERLAND, School of Chemistry, The University of Manchester. "Exploratory Studies to Investigate a Linked Prebiotic Origin of RNA and Coded Peptides".
- Wednesday 11th January: PROFESSOR A. VLCEK, Department of Chemistry at Queen Mary, University of London. "Ultrafast Excited-State Processes of d6-Metal Carbonyl-Diimine Complexes: From Excitation to Photochemistry".
- Wednesday 8th February PROFESSOR HOWARD M. COLQUHOUN, School of Chemistry, University of Reading. "The Message in the Molecule: Probing Polymer Sequences with a Molecular Tweezer".
- Wednesday 15th February: DR DAVID KLENERMAN, University Chemical Laboratories, University of Cambridge. "New biophysical tools to study biomolecules and living cells based on single molecule fluorescence and a scanned nanopipette."
- Wednesday 1st March: PROFESSOR STEPHEN MANN, School of Chemistry, University of Bristol. " Beyond Nano - the Chemistry of Emergence".
- Monday 15th May : DR. KIYOTAKA ONITSUKA, The Institute of Scientific and Industrial Research,Osaka University, Japan. "Precise synthesis and properties of organometallic dendrimers".

